Method for Quantitative Evaluation of Kinetic Constants in Olefin Polymerizations. I. Kinetic Study of a Conventional Ziegler–Natta Catalyst Used for Propylene Polymerizations

VÁLTER MATOS,[1] ANTÔNIO G. MATTOS NETO,[1] JOSÉ CARLOS PINTO[2]

[1] Polibrasil Resinas SA, Rua Hidrogênio, 1404, Complexo Petroquímico de Camaçari, Camaçari, 42810-000 BA, Brazil

[2] Programa de Engenharia Química/COPPE, Universidade Federal do Rio de Janeiro, Cidade Universitária, CP:68502, Rio de Janeiro, 21945-970 RJ, Brazil

Received 21 January 2000; accepted 7 June 2000

ABSTRACT: A method for quantitative evaluation of kinetic constants in Ziegler–Natta and metallocene olefin polymerizations is presented. The method comprises some fundamental steps, which include the initial design of a statistical experimental plan, the execution of the designed experiments, the development of simple mathematical models to describe the polymerization, and the estimation of kinetic parameters from available rate, gel permeation chromatography, and NMR data. The method is applied to the slurry propylene polymerization, using a conventional first generation Ziegler–Natta catalyst, in a lab-scale polymerization reactor. It is shown that the proposed method allows the successful interpretation of experimental olefin polymerization data and the quantitative evaluation of kinetic constants, which can be inserted into a process simulator to provide an accurate picture of actual industrial plant behavior.
 J Appl Polym Sci 79: 2076–2108, 2001

Key words: Ziegler–Natta; catalyst; propylene; polymerization; estimation; kinetic constant

INTRODUCTION

Production of polyolefins is a multibillion business, responsible for the production of more than 80 million metric tons of polymer resins and moving approximately 50 billions of U.S. dollars worldwide[1] per year. New polyolefin plants are being built in many places of the world and new projects are under development. Due to all this engineering activity and the relatively high complexity of the kinetic behavior and operation of polyolefin plants, decision making sometimes relies on simulations performed with complex mathematical models of the polymerization process. For this reason, a significant number of papers has been published regarding modeling and simulation of olefin polymerization reactors[2–6] in the last two decades. Some of these models have been implemented and are available in commercial process simulators, such as Polyred (Hyprotech), Polymers Plus (Aspen), Pro II (Simulation Science), and Simulpol (Polibrasil).

Although the free-radical solution technology is used to produce low-density polyethylene (LDPE) in industrial scale,[2] polyolefin production is based mostly on the olefin coordination polymerization, using Ziegler–Natta[3–5] and metallocene catalysts.[6] In these processes, catalyst and

Correspondence to: José Carlos Pinto (E-mail: pinto@peq.coppe.ufrj.br).
Contract grant sponsor: Polibrasil Resinas SA

Journal of Applied Polymer Science, Vol. 79, 2076–2108 (2001)

process are extremely interdependent and the process cannot be understood without the proper understanding of the catalyst behavior and vice-versa. The number of different Ziegler–Natta and metallocene catalysts used both commercially and in research activities is enormous,[7] and virtually all sorts of chemical and kinetic behavior have already been described for these catalysts. In spite of that, the number of consistent sets of kinetic constants for typical Ziegler–Natta and metallocene catalysts is extremely small. This means that, unless one has access to proprietary information, simulations (thus, plant design and optimization) carried out with mathematical models and process simulators have to rely greatly on guesses and on the feeling of the engineer.

The kinetics of polymerization of olefins through coordination polymerization is very complex for many reasons. First, the catalyst may be seen as a mixture of different active species, generated by a number of side reactions that may occur during the catalyst preparation and by the intimate interaction of the catalyst sites with the reaction environment.[8,9] Second, chain transfer reactions, used to control the molecular weight distribution (MWD), are promoted by different chain transfer agents[10] (monomers, hydrogen, cocatalysts) and the importance of these reaction steps are different for each catalyst species. Besides, usually the catalyst is not stable and the catalyst stability is influenced by the reaction environment and is different for each particular catalyst system analyzed[11]. Finally, mass transfer limitations may be present during the polymerization, causing changes of product properties and process performance.[12,13]

For all the reasons presented, different kinetic aspects have to be analyzed simultaneously, if the global catalyst performance is to be understood. This may lead to very large and complex kinetic models that depend on hundreds of kinetic constants, which most of the times are not available for the process engineer.[14] Besides, even when some kinetic parameters are available in published material, most of the times they cannot be used with confidence by the process engineer, because kinetic parameters depend on the catalyst system, the operation conditions (including the feedstock quality), and the particular kinetic mechanism used to model the kinetics of polymerization. Therefore, for process simulators to be used successfully at plant site, some sort of experimental support must be provided.

A recent review carried out by one of the authors[15] shows that the vast majority of the papers related to the kinetic behavior of Ziegler–Natta and metallocene catalysts is concerned with qualitative mechanistic aspects of the polymerization kinetics and does not give much attention to the quantitative evaluation of the kinetic constants. When kinetic constants are provided, generally research efforts are concentrated on a small subset of the whole polymerization phenomena, such as the evaluation of the kinetic constants that describe the chain transfer kinetics for hydrogen for a particular catalyst system. Therefore, most of the times the global performance of the catalyst system cannot be captured from the available data.

The main objective of this manuscript is to present a method for quantitative evaluation of kinetic constants in Ziegler–Natta and metallocene olefin polymerizations. The method comprises some fundamental steps, which include the initial design of a statistical experimental plan, the execution of the designed experiments, the development of simple mathematical models to describe the polymerization, and the estimation of kinetic parameters from available rate, gel permeation chromatography (GPC), and nuclear magnetic resonance (NMR) data. The method is applied to the slurry propylene polymerization, using a conventional first generation Ziegler–Natta catalyst, in a lab-scale polymerization reactor. The kinetic mechanism used as a support for parameter estimation is very simple, which does not mean that more complex mechanisms cannot be used. The kinetic mechanism used as support comprises the well-known activation, propagation, chain transfer, and decay steps, which is able to describe the most important kinetic phenomena observed at plant site and used to monitor and control the plant operation. If more complex kinetic mechanisms are to be used,[14] then the set of kinetic parameters obtained with the proposed method may be used as a fair initial guess for more involving parameter estimation procedures.

Although more advanced Ziegler–Natta and metallocene catalysts are known and used for propylene polymerizations, conventional first and second generation Ziegler–Natta catalysts are still used to produce around 20% of the polypropylene produced in the world. These old catalysts and technologies are still expected to survive for at least one more decade,[16] given the current trends of the business and the flexible design of

the polymerization plants built for polypropylene production with these catalysts. Therefore, the proper quantitative understanding of the kinetics of first and second generation Ziegler–Natta catalysts may delay the disappearance of the older technologies and help the improvement and retrofitting of existing polymerization plants. Besides, conventional Ziegler–Natta catalysts may be regarded as benchmarks of the propylene polymerization process. For all these reasons, first generation Ziegler–Natta catalysts are used in this study.

It is shown here that the proposed method allows the successful interpretation of experimental olefin polymerization data and the quantitative evaluation of kinetic constants, which can be inserted into a process simulator to provide an accurate picture of actual industrial plant behavior.

EXPERIMENTAL

Catalyst Preparation

The polymerization catalyst used in all experiments is a conventional first generation cocrystallized $TiCl_3$–$AlCl_3$ catalyst, suspended in an inert organic diluent. The catalyst preparation follows the well-known two-step procedure, where $TiCl_4$ is reduced by alkyl-aluminum compounds and then is precipitated at ambient temperatures.[17,18]

A solution of isododecane (Bayer) and $TiCl_4$ (Titanium Chloride), containing two parts of isododecane and one part of $TiCl_4$ in volume, is prepared in a 2-L jacketed glass reactor, under nitrogen atmosphere, at 30°C and atmospheric pressure. The solution temperature is then reduced to 0°C with a cold bath. A second solution containing 25% in mass of an equimolar mixture of diethyl-aluminum (DEAC, Akzo) and methyl-ethyl-aluminum (MEAC, Akzo) in isododecane is added slowly to the $TiCl_4$ solution, under mild agitation conditions, so that the final aluminum/titanium molar ratio be equal to a specified value (A/T ratio) after 8 h of continuous feed. After keeping reactor preparation conditions constant for 15 min, reactor temperature is slowly and linearly increased until 110°C for a period of 1 h and 30 min. The catalyst solution is kept at constant preparation conditions for additional 8 h and is finally cooled down to ambient temperature. The precipitated solid material is then filtered and washed with cold isododecane, for removal of soluble species. The final catalyst is believed to present

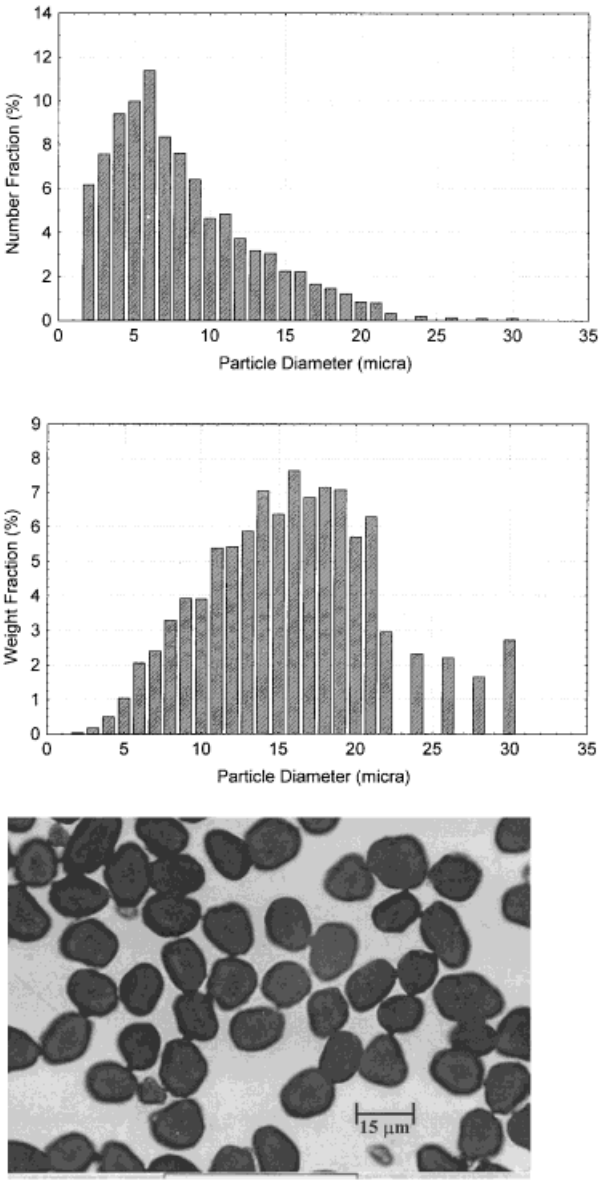

Figure 1 Typical particle size distribution (a) and morphology (b) obtained for catalyst powder.

the general chemical formula $TiCl_3.0.33AlCl_3$. The catalyst is then stored in isododecane suspensions, with a solid content of approximately 10%. The typical particle size distribution obtained is presented in Figure 1(a). An optical micrograph of the final catalyst particles is shown in Figure 1(b). It may be observed that catalyst particles are fairly uniform and present regular shape and low porosity.

Polymerization Reaction

Polymerization reactions are carried out in a standard 2-L stainless-steel Paar reactor,

equipped with internal coils for refrigeration and temperature control. The reaction mixture is stirred continuously with a speed-controlled stirrer, equipped with a three-blade turbine impeller. Heat is provided by an external heating-mantle. Reactor temperature and pressure are monitored and controlled in-line. The propylene feed line is equipped with a mass flow meter (Aalborg), which measures propylene feed rates continuously. All reaction variables are stored in a standard PC process computer, which is connected with the reactor instruments through a data acquisition board (Strawberry). Data acquisition and control algorithms are implemented with the software *Workbench 3.0* (Strawberry), which manipulates the data acquisition board.

Before reaction is started, the reactor is blown with nitrogen (high purity polymerization grade provided by COPENE) to remove oxygen and humidity. The reactor is then charged with 1 L of isododecane under nitrogen atmosphere, at ambient temperature and atmospheric pressure. The diluent is then heated slowly until the polymerization temperature, at constant pressure. The propylene feed valve is open and propylene (high purity polymerization grade provided by COPENE) is fed continuously until equilibrium is reached (the mass flow meter indicates no feed) at the specified reaction pressure. A surge tank is used in the feed line, to regulate the reactor pressure at the desired value and allow the continuous feed of monomer to the reactor. A small 100 mL stainless steel vessel is installed between the surge tank and the reactor vessel to allow the controlled feed of hydrogen (99.5% pure polymerization grade, provided by White Martins). When hydrogen is added to the reaction environment, the small vessel is fed with hydrogen until the specified hydrogen pressure is reached, before the monomer feed is started. Then, as the hydrogen feed lines are closed and the monomer feed lines are open, hydrogen is pushed into the reactor vessel by the flowing monomer feed. After reaching equilibrium conditions, the specified amounts of catalyst and cocatalysts are added to the reactor vessel through a high precision pneumatic metering pump (Polibrasil). About 50% of the cocatalyst is fed before the catalyst, to remove possible catalyst poisons from the diluent. The remaining 50% of cocatalyst is added to the catalyst suspension before feeding.

As soon as catalyst is added, the reaction begins. Monomer feed flow rates are recorded continuously and are assumed to be equal to the reaction rates, as mass transfer resistance is negligible at reaction conditions (independent experimental studies not shown here indicate that polymer yield does not depend on the agitation speed and that catalyst activity does not depend on the catalyst concentration in the whole range analyzed in this manuscript). The polymerization reaction is stopped after reaching the specified batch time by adding 10 mL of isopropyl alcohol into the reactor vessel. The reactor is then cooled down to ambient temperature and the suspended solids are removed through filtration. The solid material and samples of 100 mL of the liquid phase are dried under vacuum. The solid residual of the liquid phase (*solubles*: polymer mass fraction extracted by diluent—% weight) and the polymer powder are then weighed and characterized.

Polymer Characterization

The polymer characterization procedures used in this work are the XO (polymer mass fraction extracted by boiling xylene—% weight), the GPC, and the NMR analysis.

The XO analysis is generally used to allow a rough evaluation of the total atactic polypropylene content of the polymer resin. First, 2 g of polymer are dissolved in 100 mL of boiling xylene, under continuous agitation. The solution is then left at boiling conditions for around 15 min. Afterward, the solution is cooled down to 25° C. After 30 min of rest, the solution is filtered. The solid and liquid phases are then dried under vacuum. The solid residual of the liquid phase (XO) and the solid powder (insolubles) are then weighed and characterized through GPC and NMR.

The GPC analysis were carried out in a Waters-150CV chromatographer, equipped with 4 Ultra-styragel separation columns (10^3–10^4–10^5–10^6) from Waters. Polymer samples were dissolved in 1,2,4-trichlorobenzene (TCB) and measurements were performed at 140°C. Polystyrene standards from Polymer were used to calibrate the GPC.

The ^{13}C NMR analysis were carried out in a Varian Inova-300 equipment, at frequencies of 75.4 MHz. The time interval used for analysis was equal to 10 s. Polymer samples were dissolved in TCB and measurements were performed at 95°C. Deuterated benzene was added to the polymer solution to allow the homogenization of the magnetic field and to improve the resolution

of the spectral analysis. Polymer characterization was based on the methyl (CH_3, 20–22 ppm) and methylenic (CH_2, 45–47 ppm) signals, as described in the literature.[19,20]

Experimental Design

Seven independent variables were selected for this study. The first variable is the reaction pressure ($6 < P < 8$ Kgf/cm^2 · g), which is an important variable for monitoring of plant operation and control of the monomer concentration. The second variable is the hydrogen concentration, evaluated as the hydrogen pressure ($0 < P_H < 1$ Kgf/cm^2 · g) inside the small vessel before the monomer feed is started. Hydrogen is known for exerting major influence upon Ziegler–Natta propylene polymerization reactions.[14] The third variable is reaction temperature, which is allowed to vary within the interval $50 < T < 70$°C. The forth variable is the catalyst concentration, evaluated as the total amount of titanium added to the reactor vessel ($200 <$ [Ti] < 400 mg/L). The fifth variable is the amount of alkyl-aluminum added to the reaction environment during catalyst preparation, evaluated as the Al/Ti molar ratio ($0.90 < A/T_1 < 1.12$). This variable is believed to influence the amount of solubles and the XO produced during the polymerization.[21,22] The sixth variable is the batch time ($1 < t < 3$ h), included in the experimental design to allow the evaluation of the well-known catalyst decay.[11] The seventh variable is the amount of alkyl-aluminum added to the reaction environment during polymerization, evaluated as the Al/Ti ratio ($1.4 < A/T_2 < 2$), expected to influence both catalyst activity and the average molecular weight of the final polymer resin.[23] The experimental ranges selected in all cases are in accordance with actual industrial operation conditions. The ranges are narrow on purpose, in order to allow the investigation of effects caused by variable fluctuations within usual operation constraints and must not be regarded as an experimental drawback.

To analyze the main effects of the selected variables upon the polymerization results, a minimum Taguchi experimental design[24] was proposed. The minimum Taguchi design allows the evaluation of main variable effects independently from each other, provided that variable interactions are not important. This is certainly a false assumption in this case, as the kinetics of polymerization introduces variable interactions between many of the variables analyzed. For instance, polymerization rates are expected to follow rate equations that are similar to

$$R_{\mathrm{Pol}} \approx k_0 \exp\left(\frac{-\Delta E}{RT_k}\right) P_M[Cat] \qquad (1)$$

where R_{pol} is the polymerization rate, T_k is the absolute reactor temperature, P_M is the partial monomer pressure, $[Cat]$ is the catalyst concentration, R is the universal gas constant, and k_0 and ΔE (activation energy) are parameters. Equation (1) shows a strong third-order interaction between temperature, partial monomer pressure, and catalyst concentration. Additional rate expressions are expected to introduce interactions between time, cocatalyst concentration, and hydrogen concentration with the other three variables described above. If these interactions are to be evaluated independently, then a much larger number of experiments would have to be carried out, which is not possible due to time and cost limitations. Therefore, the minimum Taguchi design is used here mostly for geometric reasons (uniform distribution of experiments over the experimental grid), as the main effect analysis may be of limited value.

All experiments were made in duplicates, to allow the evaluation of experimental consistency. Results were regarded as valid when duplicates led to similar polymer productivities, as it is known that Ziegler–Natta catalysts are very sensitive to impurities.[25] The most expensive analysis, however, were carried out only for a smaller subset of the whole experimental set. Additional central experiments were added to the experimental plan to allow the evaluation of possible nonlinear effects. Finally, a set of *standard* polymerization conditions, which are usually performed in the lab to test catalyst performance, was added to the experimental plan to check for changes of the feed stock properties during this experimental study. Although the central experimental conditions might be used with this objective, the standard polymerization conditions were selected for practical commercial reasons that are beyond the objectives of this article.

All experiments were ordered at random, to minimize the influence of possible extraneous effects. Experimental conditions and results obtained are shown in Tables I and II. Some of the results obtained for solubles could not be presented because the total amount of dry polymer obtained was too small. XO values were not eval-

Table I Experimental Design

Experimental Tag	Order	P (Kgf/cm^2 · g)	P_H (Kgf/cm^2 · g)[a]	T (°C)	[Ti] (mg Ti/L)	A/T_1	t (h)	A/T_2
H0	1	7	1	65	200	0.90	2	2
H0	15	7	1	65	200	0.90	2	2
H0	28	7	1	65	250	0.90	2	2
H0	37	7	1	65	250	0.90	2	2
H1	6	6	0	50	200	0.90	1	1.4
H1	9	6	0	50	200	0.90	1	1.4
H2	31	6	1	70	400	1.12	1	1.4
H2	59	6	1	70	400	1.12	1	1.4
H3	8	6	1	70	200	0.90	3	2
H3	10	6	1	70	200	0.90	3	2
H4	32	6	0	50	400	1.12	3	2
H4	56	6	0	50	400	1.12	3	2
H5	29	8	0	70	200	1.12	1	2
H5	58	8	0	70	200	1.12	1	2
H6[b]	13	8	0	70	400	0.90	2.5[c]	1.4
H7	57	8	1	50	200	1.12	3	1.4
H7	60	8	1	50	200	1.12	3	1.4
H8	11	8	1	50	400	0.90	1	2
H8	12	8	1	50	400	0.90	1	2
H9	34	7	0	60	300	1.01	2	1.7
H9	35	7	0	60	300	1.01	2	1.7
H9	55	7	0	60	300	1.01	2	1.7
H9	36	7	0	60	300	1.01	2	1.7
H10	38	7	1	60	300	1.01	2	1.7
H10	39	7	1	60	300	1.01	2	1.7

[a] 0 represents absence of hydrogen in the feed stream.
[b] Reaction was not repeated because it led to too much polymer.
[c] Reaction was interrupted for excess of polymer.

uated for all polymer samples, due to the high costs of the XO analysis (XO analysis is too long), but at least one value is available for each experimental condition. Such experimental constraints are very common in an industrial lab and the experimental strategy must be flexible enough to accommodate possible lack of data.

DATA ANALYSIS

The first important piece of information presented in Table II regards the experimental error. According to Table II, the standard errors for polymer yield, solubles and XO are respectively equal to 20 g, 0.28%, and 0.12% (experiment 15 is an outlier for XO), which means that polymer yield, solubles and XO are accurate within ±40 g, ±0.60 %, and ±0.25%, respectively, with confidence of about 95%. These numbers are very important because they will be used for analysis of model adequacy and statistical significance in the following subsections. Typical output values for catalyst activity, solubles and XO are respectively 520 ± 100 g/gTi h, 1.01 ± 0.33 %, and 4.8 ± 0.6 % with confidence of 95%.

Correlation and Main Effect Analysis

Table III shows the correlation coefficients, or alternatively the main linear effects, among the variables analyzed. It can be seen in the first six lines and columns of Table III that correlation coefficients between pairs of independent variables are always very small due to the experimental design implemented. This illustrates that the minimum Taguchi design allows the independent analysis of individual linear effects of independent variables upon the final polymerization results.

Reaction temperature is the most important variable analyzed, given the large and significant

Table II Experimental Results

Experimental Tag	Order	[Ti][a] (mg Ti/L)	Polymer Yield (g)	Average Activity (g/g Ti h)	Solubles (weight %)	XO (weight %)
H0	1	212.7	299	703	0.800	4.23
H0	15	210.3	317	754	1.120	3.33
H0	28	248.6	353	730	1.100	4.21
H0	37	253.0	372	726	1.060	4.23
H1	6	200.7	54	269	0.800	4.32
H1	9	201.4	59	293	0.140	3.98
H2	31	400.1	307	767	1.610	4.58
H2	59	401.0	340	848	1.470	
H3	8	200.7	457	759	2.340	4.59
H3	10	201.4	495	820	2.380	4.43
H4	32	400.1	318	265	0.260	3.43
H4	56	410.0	338	275		
H5	29	201.5	214	1062	0.840	6.67
H5	58	201.7	211	1046	1.670	
H6	13	401.1	860	858		6.48
H7	57	199.6	145	242	0.700	7.69
H7	60	200.6	156	259	0.840	
H8	11	401.8	172	428	0.200	4.53
H8	12	400.7	195	487	0.290	4.65
H9	34	299.2	358	648		4.20
H9	35	303.7	355	585		
H9	55	301.0	363	603	0.580	
H9	36	308.6	371	601		
H10	38	296.4	452	763		
H10	39	297.5	426	716		6.67

[a] Actual catalyst concentration used in the experiments.

correlation coefficients observed for polymer yield, catalyst activity, and total amount of solubles. As expected, temperature causes the increase of yield variables and a selective increase of soluble material, indicating the increase of the polymerization activity of catalyst sites, specially of the atactic catalyst sites.[21,22] Surprisingly, XO values apparently do not depend on reaction temperature, which seems to indicate that variations of the amounts of the XO and soluble fractions are

Table III Correlation Coefficients Among Polymerization Variables

	P	P_H	T	A/T_1	t	A/T_2	[Ti]	Yield	Activity	Solubles	XO
P	1.00	0.06	−0.06	0.05	−0.11	0.07	−0.08	−0.03	0.15	−0.35	0.58[a]
P_H	0.06	1.00	0.15	−0.22	0.09	0.11	−0.08	0.01	0.11	0.32	−0.01
T	−0.06	0.15	1.00	−0.05	−0.10	0.17	−0.14	0.56[a]	0.93[a]	0.79[a]	0.08
A/T_1	0.05	−0.22	−0.05	1.00	0.08	−0.24	0.19	−0.19	−0.04	0.02	0.42
t	−0.11	0.09	−0.10	0.08	1.00	0.11	−0.11	0.42[a]	−0.27	0.26	0.12
A/T_2	0.07	0.11	0.17	−0.24	0.11	1.00	−0.05	0.07	0.28	0.13	−0.38
[Ti]	−0.08	−0.08	−0.14	0.19	−0.11	−0.05	1.00	0.32	−0.11	−0.28	−0.04
Yield	−0.03	0.01	0.56[a]	−0.19	0.42[a]	0.07	0.32	1.00	0.49[a]	0.66[a]	0.17
Activity	0.15	0.11	0.93[a]	−0.04	−0.27	0.28	−0.11	0.49[a]	1.00	0.63[a]	0.16
Solubles	−0.35	0.32	0.79[a]	0.02	0.26	0.13	−0.28	0.66[a]	0.63[a]	1.00	−0.02
XO	0.58[a]	−0.01	0.08	0.42	0.12	−0.38	−0.04	0.17	0.16	−0.02	1.00

[a] Indicates that value is significant with confidence of 95%

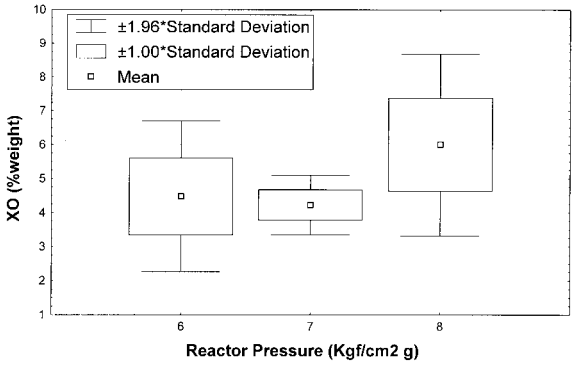

Figure 2 Box-Whisker plot of XO values.

governed by different physicochemical phenomena.

It is interesting to observe that reactor pressure and partial hydrogen pressure do not seem to exert a significant impact upon the polymerization, which is difficult to explain, as reaction rates are expected to be of first order in respect to monomer and hydrogen is known to cause increase of reaction rates.[14] However, given the large influence of temperature on the final polymerization results, final conclusions must not be sought at the moment. The XO content, however, seems to depend on reactor pressure to some extent. If Figure 2 is analyzed, though, it can be seen that significant XO fluctuation, which cannot be explained by the known experimental error, is observed within each individual pressure group. Therefore, the effect of P upon the final XO value is doubtful.

Table III shows that t causes a significant increase of polymer yield and does not influence the other variables significantly. This may be explained in terms of the catalyst activity. As first and second generation Ziegler–Natta catalysts present high stability, the concentrations of active catalyst sites remain almost constant throughout the polymerization batch, which causes t to be of minor importance to explain variations of polymer quality and catalyst productivity.

It is intriguing to observe that remaining catalyst variables do not seem to exert any influence upon the final quality of the polymer resin and catalyst productivity. Polymer yield is assumed to be of first order in respect to catalyst concentration and solubles and XO are assumed to be functions of the A/T ratio used during both the catalyst preparation and the polymerization reaction.[21–23] These effects may be due do the large influence of temperature upon the polymerization results and due to the narrow ranges of variation of the catalyst variables, as imposed by plant operation constraints.

In order to evaluate the quality of the previous assumptions, a simple empirical model is developed for polymer yield in the form

$$\text{Yield} = \exp\left(A_0 + \frac{B_0}{T_K}\right) P_M[\text{Ti}]t(1 + cP_H) \quad (2)$$

$$A_0 = 12.65; \quad B_0 = -5080; \quad c = 0.163$$

where T_k is the absolute temperature in K and all other variables are used as defined before. The correlation between experimental and simulation results obtained in this case is equal to 96% and may be regarded as excellent. Experimental and simulation results are shown in Figure 3.

Equation (2) indicates that the polymerization activity can increase 15% in the presence of hydrogen in the range analyzed, which is very significant in an industrial environment. However, when c is made equal to zero and the other parameters are estimated, the correlation coefficient obtained is equal to 94%, which means that there is a huge uncertainty regarding the hydrogen effect upon the catalyst activity. This uncertainty led us to design an additional set of experiments, shown in Table IV. When eq. (2) is applied to the experimental data presented in Table IV, c is shown to be equal to 0.12 $(\text{Kgf/cm}^2)^{-1}$, which agrees extremely well with the results presented previously and confirms that hydrogen enhances catalyst activity considerably. Experimental and simulation results are shown in Figure 4.

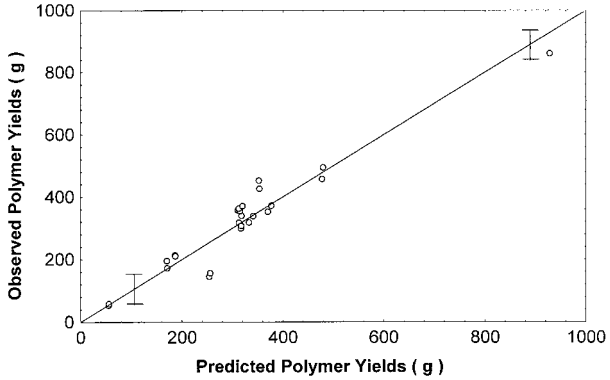

Figure 3 Comparison between predicted and observed polymer yields. (Vertical bars indicate the experimental error.)

Table IV Experimental Conditions and Results for the Hydrogen Effect Study

Experimental Tag	Order	P (Kgf/cm^2 · g)	P_H (Kgf/cm^2 · g)[a]	[Ti] (mg Ti/L)	t (h)	Polymer Yield (g)	Average Activity (g/g Ti h)
HY0	3	6.0	0.0	213.7	2	304	711.0
HY0	7	6.0	0.0	195.1	2	262	671.5
HY1	1	6.5	0.5	196.5	2	351	893.0
HY1	14	6.5	0.5	199.8	2	365	913.0
HY2	10	7.0	1.0	205.8	2	433	1052.0
HY2	8	7.0	1.0	199.8	2	378	946.0
HY2	5	7.0	1.0	200.1	2	381	952.0
HY3	11	8.0	2.0	204.7	2	475	1160.0
HY3	6	8.0	2.0	200.6	2	460	1146.5
HY4	9	7.0	1.0	202.5	3	471	775.3
HY4	2	7.0	1.0	195.6	3	475	809.3
HY5	4	7.0	1.0	192.4	4	603	783.5
HY6	13	7.0	1.0	125.1	4	389	777.5
HY6	12	7.0	1.0	121.4	4	370	762.0

[a] 0 represents absence of hydrogen in the feed stream.

It is not necessary to analyze the average catalyst activity as a function of the independent variables because it is obtained both theoretically and experimentally as the ratio between the total polymer yield and the product of catalyst feed and polymerization time. It is important to observe that it is not needed to take the A/T ratio into consideration to reproduce the experimental catalyst activity results, which probably indicates that the experimental ranges analyzed for both A/T_1 and A/T_2 are too narrow for any significant effect to be observed, given the large influence of temperature upon the final results. (This is confirmed by independent observation of plant behavior at Polibrasil Resinas SA, Camaçari— BA, Brasil.)

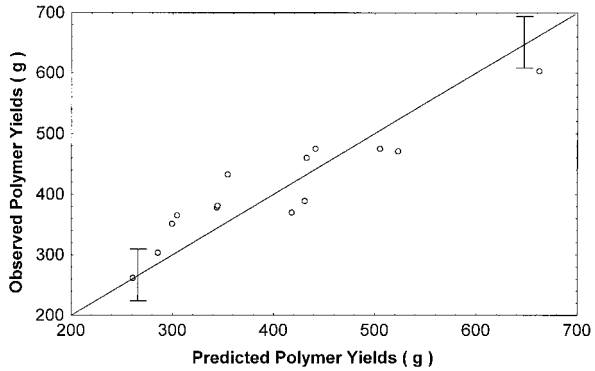

Figure 4 Comparison between predicted and observed polymer yields for the hydrogen study. (Vertical bars indicate the experimental error.)

Assuming that solubles are produced in atactic catalyst sites that behave very similarly to the other ones, as Table III indicates that the correlation coefficient between the total polymer yield and the total amount of solubles is positive and significant, it is possible to write

$$\text{Solubles} = \exp\left(A_0 + \frac{B_0}{T_k}\right)(1 + cA/T_1) \qquad (3)$$

$$A_0 = 34.51;\ B_0 = -11313;\ c = -0.618$$

where the first exponential term takes into account differences of the propagation constants for production of the soluble and insoluble fractions, and the second linear term is a function that separates two blocks of experimental conditions, depending on the values of the A/T ratio used during catalyst preparation. Results obtained are shown in Figure 5 and lead to a correlation coefficient of 86% between experimental and calculated results, which may be regarded as very good, given the occurrence of relatively large experimental errors. The blocking procedure was also performed for the other independent variables, but results obtained were always worse than the ones presented.

Equation (3) shows that the catalyst preparation procedure may be very important for the correct interpretation of the production of the soluble fraction, even when narrow ranges of opera-

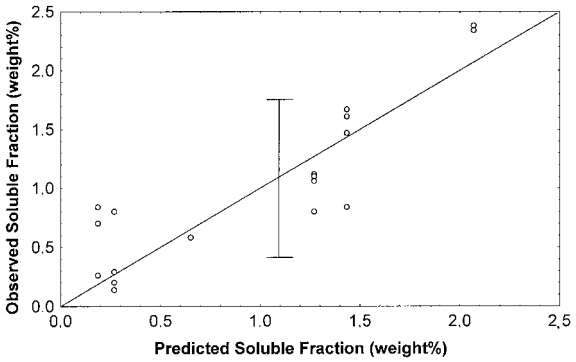

Figure 5 Comparison between predicted and observed soluble polymer fractions. (Vertical bar indicates the experimental error.)

tion conditions are analyzed. According to eq. (3), the increase of the A/T ratio used for preparation leads to reduction of the total amounts of solubles produced. At higher temperatures, the reduction of solubles is close to 1% when A/T_1 is allowed to vary within the experimental range analyzed, which may be very significant for actual plant operation. The activation energy obtained for solubles production, however, seems to be too high. As simulation results are worsened significantly when the activation energy is diminished, eq. (3) is left as it is. It is quite probable that thermodynamic equilibrium and mass transfer constraints affect the total amount of solubles obtained, as this polymer fraction is actually extracted from the polymer mass during polymerization, leading to the high activation energy of eq. (3). Available experimental results[26] show that the total amount of solubles depend on the catalyst morphology and porosity, which gives some support to this hypothesis. As internal molecular structure and morphology, such as stereoblock and molecular weight distributions, are expected to exert great influence on mass transfer and thermodynamic equilibrium constraints, it is not intended here to present a deeper discussion about this subject. However, it must be pointed out that eq. (3) allows excellent description of soluble contents at Polibrasil Resinas SA, Camaçari—BA, Brasil, during actual process operation conditions.

When the same approach used for solubles is used to develop an empirical model for XO, results obtained are not good, due to the moderate correlation between XO and reaction pressure. Besides, Table III indicates that the sources of variation for XO are different from the cases analyzed before, as the correlation coefficients between XO and polymer yield and XO and solubles are small and not significant. When the monomer pressure is used to describe the XO fluctuations, Equation (4) can be obtained:

$$\mathrm{XO} = (a + bA/T_1 + cA/T_2)\exp\left(\frac{B_0}{T_k}\right)P_M^d \quad (4)$$

$$B_0 = -590; \quad a = 1.88; \quad b = 1.78;$$

$$c = -0.76; \quad d = 1.32$$

where a variable blocking strategy was used as before and the order in respect to the monomer partial pressure was allowed to vary. Experimental and calculated results are shown in Figure 6, where it can be seen that experimental errors cannot be blamed for the model deviations observed.

As eq. (4) shows, the monomer effect is very important to describe XO variations, although temperature does not seem to be of much importance. If one thinks that XO is the ratio between two polymer fractions, then it seems plausible to admit that the catalyst activities for both fractions have approximately the same activation energy and that the kinetics for the XO fraction is approximately of order 2 in respect to monomer. [Actually, results are almost the same when d is made equal to 1 in eq. (4). In this case, the other parameters become: $B_0 = -578$; $a = 3.25$; $b = 3.29$ and $c = -1.32$.] This result can be explained in terms of trigger mechanisms,[27,28] if it is assumed that the metal–monomer complex can be triggered by another monomer molecule to give

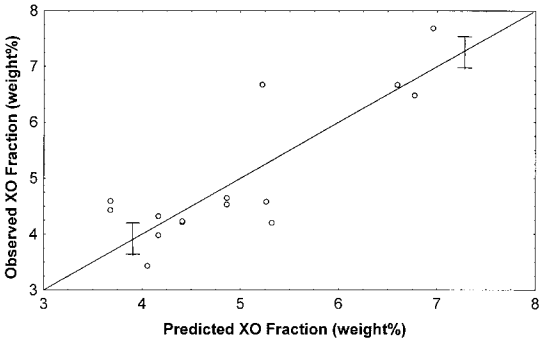

Figure 6 Comparison between predicted and observed XO polymer fractions. (Vertical bars indicate the experimental error.)

birth to a polymer chain defect, as the XO fraction is composed of polymer chains with low degree of isotacticity, as shown in the following sections. This text does not intend to provide conclusions about this subject, though. It is also important to emphasize that if d is made equal to zero in eq. (4), then the correlation coefficient between model predictions and experimental results is always below 0.40, which seems to indicate that monomer concentration is indeed important to describe XO fluctuations.

Equation (4) also shows that the XO fraction is influenced significantly by the catalyst preparation procedure and by the amount of alkyl-aluminum added to the reaction environment. As XO is expected to increase with A/T_1 and to decrease with A/T_2, variations of catalyst preparation conditions can be corrected at plant site through manipulation of the alkyl-aluminum concentration inside the reactor. This is confirmed by independent observation of plant behavior at Polibrasil Resinas SA, Camaçari—BA, Brasil, and shows that the alkyl-aluminum species play very different roles during catalyst preparation and polymerization. It is also interesting to observe that the A/T ratio causes opposite effects upon the XO and soluble fractions, which seems to confirm that different physicochemical phenomena govern the production of these polymer fractions.

GPC Deconvolution

More detailed information regarding the catalyst behavior can be obtained from the MWD of the final polymer, obtained through GPC analysis. If MWDs are available, then information about the number of catalyst site types and the kinetic parameters of the kinetic steps that control the MWD can be recovered, as described below.

Mathematical Modeling

If the polymerization conditions are kept constant throughout the polymerization batch and if it is assumed that the catalyst is a mixture of a finite number of different types of catalyst sites, then the MWD of the final polymer obtained may be described as the sum of a finite number of Schulz–Flory distributions[29] in the form

$$\Lambda_i = \sum_{j=1}^{N} A_j q_j^{i-1} \tag{5}$$

where Λ_i is the molar concentration of polymer chains of size i in a polymer sample, A_j depends on the concentration of the catalyst site type j, and q_j (propagation probability of the particular catalyst site analyzed) depends on the polymerization mechanism. For numerical reasons, it is convenient to present eq. (5) in a normalized form. Based on eq. (5), the total mass of polymer produced by the catalyst site type j in the polymer sample can be computed as

$$M_j^T = \mathrm{PM} A_j \sum_{i=1}^{\infty} i q_j^{i-1} = \mathrm{PM}\,\frac{A_j}{(1-q_j)^2} \tag{6}$$

where M_j^T is the total mass of polymer produced at the particular catalyst site analyzed and PM is the molecular weight of the monomer species. Therefore, eq. (5) becomes

$$\Lambda_i = \sum_{j=1}^{N} \frac{M_j^T (1-q_j)^2}{\mathrm{PM}}\, q_j^{i-1} \tag{7}$$

which can be written in terms of the mass concentration of polymer chains of size i, M_i, as

$$M_i = \mathrm{PM} i \sum_{j=1}^{N} \frac{M_j^T (1-q_j)^2}{\mathrm{PM}}\, q_j^{i-1} = \sum_{j=1}^{N} M_j^T (1-q_j)^2 i q_j^{i-1} \tag{8}$$

Equation (8) can be written in terms of the mass fraction of polymer chains of size i as

$$M_i = \frac{\sum_{j=1}^{N} M_j^T (1-q_j)^2 i q_j^{i-1}}{\sum_{j=1}^{N} M_j^T} = \sum_{j=1}^{N} \alpha_j (1-q_j)^2 i q_j^{i-1} \tag{9}$$

where α_j is the relative activity of the catalyst site type j or the polymer mass fraction produced by the catalyst site type j. The mass fractions of the polymer chains of size between 1 and a certain arbitrary value L can then be summed to produce the cumulative molecular weight distribution as

$$F_L = \frac{\sum_{i=1}^{N} \alpha_j\{1 - q_j^L[1 + L(1 - q_j)]\}}{\sum_{j=1}^{N} \alpha_j} \quad (10)$$

where F_L is the mass fraction of polymer chains with size smaller than or equal to L.

Equation (10) is the model used in this work to represent experimental MWD obtained by GPC. The use of eq. (10) is rather convenient, as it is much easier to analyze model deviations and trends with the cumulative distribution because F_L is always a monotonic increasing function of i constrained in the interval [0,1], which provides a natural normalization interval for all polymer samples. Besides, eq. (10) allows the manipulation of numbers of similar orders of magnitude, which enhances the performance of numerical procedures. Alternative deconvolution procedures are presented in the literature for both homopolymers[30] and copolymers,[31] based on the differential form of the GPC chromatogram. Although it is not intended here to compare the numerical algorithms devised for GPC deconvolution, it is important to say that the initialization of the numerical algorithm and computation of parameter estimates were always performed much better when eq. (10) was used as the model. It seems that some numerical problems may arise when the differential form of the GPC is used as a model because the numerical iterative procedure may place parameter estimates at regions where the model is not much sensitive to parameter variations and the chromatogram signal is very close to zero. This happens at both sides of the GPC chromatogram when the differential form is used. However, if one feels more comfortable with the differential form of the GPC chromatogram, then eq. (10) may be used to generate the initial guesses for a second round of GPC deconvolutions.

Observe that the model used here contains $(2N - 1)$ parameters to be determined: $q_1, \ldots, q_N, \ldots, \alpha_1, \ldots, \alpha_{N-1}$, as

$$\sum_{j=1}^{N} \alpha_j = 1 \quad (11)$$

As polymer average molecular weights are large, parameters q_j are always very close to 1, which means that parameter estimation is very difficult if the model is written as in eq. (10), because any small perturbation of q_j leads to large modifications of the MWD. Besides, q_j is not allowed to grow above 1 or decrease below 0. For these reasons, the parameters q_j are written as

$$q_j = \exp(-\theta_j) \quad (12)$$

In this work, the deconvolution problem consists of estimating the parameters $\theta_1, \ldots, \theta_N, \ldots, \alpha_1, \ldots, \alpha_{N-1}$, in eqs. (10)–(12) in order to reproduce experimental cumulative MWDs obtained through GPC. Standard maximum likelihood parameter estimation procedures[32] are used to allow the estimation of the model parameters. The estimation routine is repeated iteratively for increasing values of N, until one (or both) of the following tolerance criteria is satisfied:

1. The model obtained leads to a computed polydispersity index that is larger than the one obtained experimentally. This heuristic procedure assumes that increasing the number of catalyst site types will not cause narrowing of the computed MWD;
2. The partial activities of some of the catalyst site types are not statistically significant, as evaluated with the standard Student t-test.[32] If the additional parameters lead to a model that is not statistically significant, it is assumed that the additional site type is not relevant for the deconvolution of the experimental MWD.

This mathematical procedure was implemented in FORTRAN for automatic deconvolution of the experimental MWD, using a standard library of maximum likelihood parameter estimation routines.[33]

Analysis of the Final Polymer Powder

The data obtained after deconvolution of some of the experimental MWD of the final polymer resin (which excludes the soluble polymer fraction, but not the XO fraction, as the XO fraction is obtained after fractionation of the final polymer resin) are shown in Table V. In all cases analyzed, no more than two site types were needed to allow the adequate description of the experimental MWD of the final polymer powder. The use of a single site type usually led to computed MWDs that were much narrower than the ones obtained experimentally, as illustrated in Figure 7, while the use of three site types always led to model parameters

Table V Deconvolution of the MWDs of Final Polymer Samples

Experimental Tag	Order	θ_1	θ_2	α_1	PMn (g/gmol)	PMw (g/gmol)	PD
H0	1						
H0	15						
H0	28						
H0	37						
H1	6						
H1	9	1.29×10^{-4}	6.08×10^{-4}	.868	218223	582261	2.668
H2	31	1.55×10^{-4}	5.61×10^{-4}	.237	90399	242779	2.686
H2	59						
H3	8	1.58×10^{-4}	6.57×10^{-4}	.549	109664	349674	3.189
H3	10	1.66×10^{-4}	6.48×10^{-4}	.555	110399	338649	3.067
H4	32	1.63×10^{-4}		1.000	257460	514920	2.000
H4	56						
H5	29	1.37×10^{-4}	5.21×10^{-4}	.839	211315	540133	2.556
H5	58						
H6	13	1.39×10^{-4}	7.40×10^{-4}	.655	121240	435169	3.589
H7	57						
H7	60						
H8	11	1.85×10^{-4}	6.31×10^{-4}	.353	88713	246094	2.774
H8	12	1.84×10^{-4}	7.77×10^{-4}	.432	80650	258602	3.206
H9	34	1.34×10^{-4}	7.38×10^{-4}	.924	233807	588710	2.518
H9	35	2.00×10^{-4}	5.76×10^{-4}	.745	142112	350753	2.468
H9	55						
H9	36	1.05×10^{-4}	7.15×10^{-4}	.942	300391	763444	2.541
H10	38	1.46×10^{-4}	6.96×10^{-4}	.533	104342	362449	3.474
H10	39	1.78×10^{-4}	7.63×10^{-4}	.324	73315	227811	3.107

which lacked statistical significance within the significance range of 95%. As shown in Figure 8, the use of two type sites makes computed and experimental MWDs almost identical in all cases analyzed, so that the third site type becomes unnecessary.

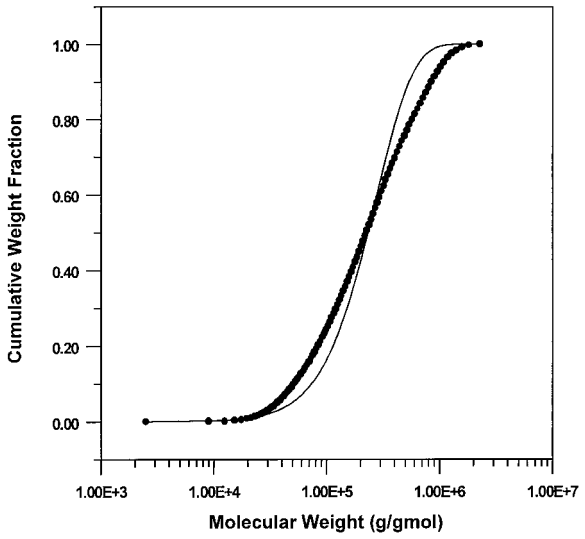

Figure 7 Deconvolution of the experimental MWD for polymerization H3–8, with the use of one site type. (●: experimental; ——: model.)

According to Table V, the MWDs of the polymer chains produced in each individual site type do not change very significantly within the range of experimental conditions analyzed, as one of the site types produces polymer chains with weight average molecular weights around 3×10^5 g/gmol while the other one produces polymer chains with weight average molecular weights around 6×10^4 g/gmol. However, the partial activities of the individual site types change considerably within the range of experimental conditions, so that the MWD of the final polymer powder may vary a lot along the experimental grid studied.

When the correlation coefficients of θ_1, θ_2, and α_1 with the other independent and dependent variables presented previously are computed, it is found that the only significant correlation are the ones that relate the hydrogen partial pressure with the partial activities of the catalyst sites. In this case, the correlation coefficient between P_H and α_1 is equal to -0.88, which means that the higher the hydrogen pressure is, the higher the

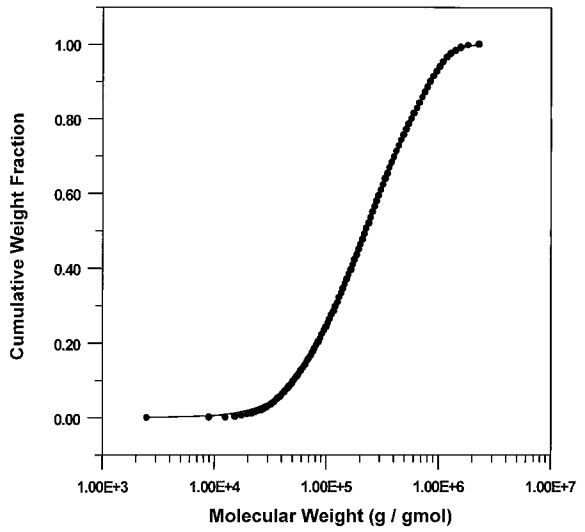

Figure 8 Deconvolution of the experimental MWD for polymerization H3–8, with the use of two site types. (●: experimental; ——: model.)

polymer weight fraction of polymer chains of low average molecular weight also is. Therefore, according to the deconvolution results, the effect of hydrogen upon the relative distribution of catalyst site types is much more pronounced than the effect of hydrogen upon individual chain transfer rates. This cannot be explained by classical kinetic mechanisms, unless it is assumed that hydrogen plays an important role for activation of catalyst sites, which is in accordance with the current interpretation of the hydrogen effect on the propylene polymerization[9,14] as being mostly caused by the reduction of the number of monomer hindered growing chains due to transfer to hydrogen. As the apparent lack of correlation between the parameters obtained through deconvolution and the other variables may be also due to the existence of strong nonlinear relationships among the variables analyzed and due to the multidimensional character of these relationships, a more fundamental analysis of deconvolution data depends heavily on the formulation of a kinetic mechanism.

In order to illustrate the approach, let us assume that chain growth is controlled by chain transfer reactions, that catalyst sites keep their intrinsic kinetic behavior along the polymerization run, that reaction orders are equal to one in respect to all reactants, and that polymerization conditions remain constant. (It must be clear that neither of these assumptions are needed, although they are useful for most practical applications and may provide excellent initial guesses for more detailed modeling of the kinetic mechanism.[14,34]) In this case, q_j can be described as

$$q_j = \frac{Kp_j[M]}{Kp_j[M] + \sum_{i=1}^{NX} Ktr_{ij}[X_i]} \tag{13}$$

where Kp_j and Ktr_{ij} are respectively the kinetic constants for propagation and the kinetic constants for chain transfer with the chain transfer agent X_i, and $[M]$ is the monomer concentration. Therefore,

$$\frac{1}{q_j} - 1 = \exp(\theta_j) - 1 = \sum_{i=1}^{NX} \frac{Ktr_{ij}}{Kp_j} \frac{[X_i]}{[M]} \tag{14}$$

In the system analyzed, chain transfer is expected to occur to monomer, to hydrogen, to cocatalyst, and also to occur spontaneously. This means that at least four different kinetic constants (eight parameters) can be estimated simultaneously to describe the variations of q_1 and q_2 along the experimental grid. The strategy used here is similar to the strategy used previously to estimate q_j, although implemented in the reverse order. Parameters are estimated simultaneously using the complete model and the least significant set of parameters is discarded. The model is then simplified and the estimation procedure is repeated. The iteration loop is halted when either all parameters are statistically significant or when a significant decrease of the correlation coefficient is observed (for instance, the correlation coefficient drops more than 10%). Results obtained are illustrated in eqs. (15)–(16) and in Figure 9.

$$\left(\frac{1}{q_1} - 1\right) \times 10^4 = \exp\left(-0.64 + \frac{312.4}{T_K}\right) + \exp\left(-12.60 + \frac{4476}{T_K}\right) \frac{P_H}{P_M} \tag{15}$$

$$\left(\frac{1}{q_2} - 1\right) \times 10^4 = \exp\left(-1.74 + \frac{1087}{T_K}\right) + \exp\left(7.66 - \frac{2434}{T_K}\right) \frac{[Cocat]}{P_M} \tag{16}$$

where pressures are given in Kgf/cm^2 · a and concentrations are given in mmol/L. As partial

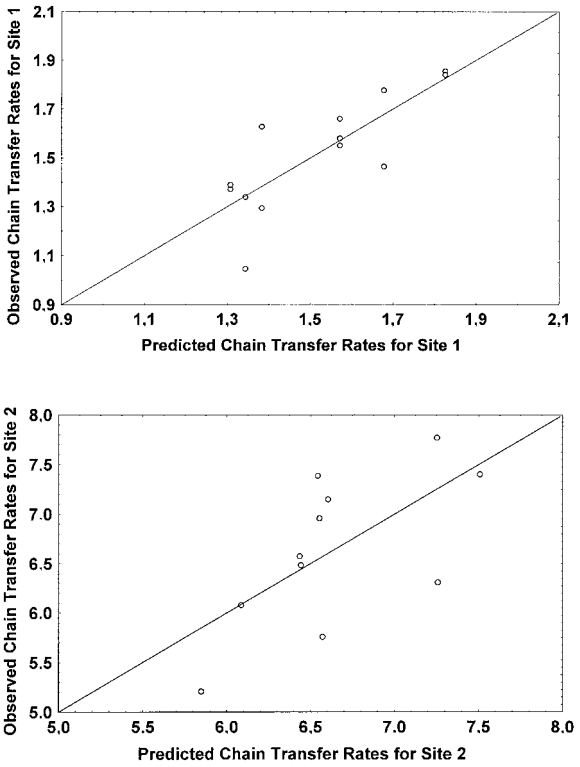

Figure 9 Observed and predicted dimensionless chain transfer rates for catalyst sites ($\times 10^4$).

pressures are used to replace concentrations, it is implicitly assumed that the Henry's law is valid and that the Henry coefficient is essentially constant in the experimental range analyzed. Both assumptions can be relaxed if more rigorous computation of monomer and hydrogen solubilities are required. However, these assumptions are believed to be very good in the cases analyzed, given the low pressures and narrow temperature ranges used experimentally.[15]

Equation (15) indicates that chain growth is controlled by chain transfer to monomer and chain transfer to hydrogen in site 1, while eq. (16) shows that chain growth is controlled by chain transfer to monomer and chain transfer to cocatalyst in site 2. These effects are the usual chain transfer effects reported in the literature for the catalyst studied.[10,35] Table VI shows the importance of the chain transfer effects at the center of the experimental grid for each site. It may be observed that chain transfer to monomer seems to be the most important chain transfer mechanism in the system. Given the relatively low activation energies in eqs. (15)–(16), this behavior is expected to be approximately the same in the whole experimental range of interest. Therefore, the key factor for control of the M_w of the final polymer powder seems to be the control of the relative amounts of sites 1 and 2 present in the reaction environment (α). However, interpretation of α is only possible if a model is available for monomer propagation, as described in the following section.

Table VI Dimensionless Chain Transfer Rates at the Center of the Experimental Grid

Chain Transfer ($\times 10^4$)	Site 1	Site 2
Monomer	1.277	3.81
Hydrogen	0.154	—
Cocatalyst	—	2.89

Analysis of the Soluble Polymer Fraction

The GPC analysis of the soluble polymer fractions obtained in the lab is very difficult, due to the very small quantities of solubles produced in each run, especially when the catalyst activity obtained is small. As from a practical point of view, the amount of the soluble fraction produced is much more important than its quality, as this fraction may be regarded as an undesired process by-product, no attempts were made to increase the production of soluble material. Results obtained are shown in Table VII. It is interesting to observe that average molecular weights are much smaller than observed previously, so that solubles are formed mostly by atactic oligomers. (The atac-

Table VII Deconvolution of the MWD of Soluble Polymer Fractions

Experimental Tag	Order	θ_1	θ_2	α_1	PMn (g/gmol)	PMw (g/gmol)	PD
H2	31	195.5×10^{-4}	1100×10^{-4}	0.586	771	2835	3.676
H3	8		32.03×10^{-4}	0.000	13132	22324	1.700
H4	32	74.93×10^{-4}	585.5×10^{-4}	0.676	1788	8040	4.496
H5	29		5.63×10^{-4}	0.000	74604	130631	1.751

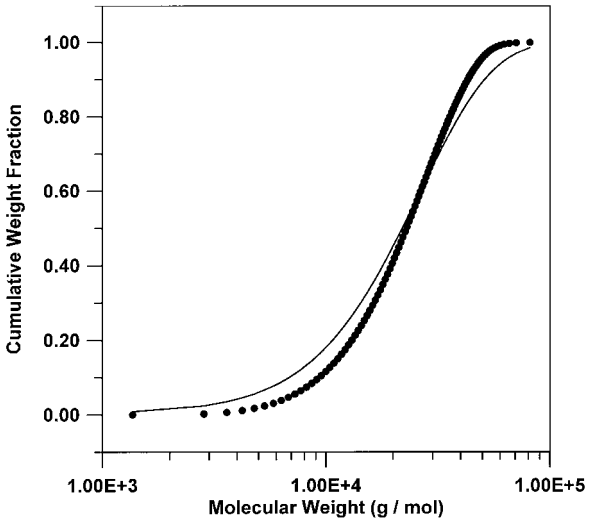

Figure 10 Deconvolution of the MWD of the soluble polymer fraction for polymerization H3–8, with the use of one site type. (●: experimental; ——: model.)

tic nature of the soluble fraction will be shown later.) Besides, Figure 10 shows that the Flory deconvolution does not lead to appropriate fitting of the experimental MWD obtained, which may also be observed through the small polydispersion indices evaluated experimentally for some samples. It is very probable that the proper understanding of the quality of the soluble fraction has to involve both the kinetics of polymerization and the equilibrium/kinetics of polymer chain extraction by solvent during the polymerization, as already discussed. Therefore, a detailed investigation of the extraction phenomena seems to be necessary if one is interested in understanding the nature of the soluble polymer fraction, which is certainly beyond the scope of this article. However, this may be regarded as a very important conclusion for process operation studies.

Analysis of the XO Fraction

As in the previous case, the GPC analysis of the XO fraction is very difficult in the lab, due to the very small quantities of XO produced in each run. As discussed previously, no attempts were made to increase the production of XO. Results obtained are shown in Table VIII. It is interesting to observe that average molecular weights of the XO fraction are smaller than the average molecular weights of the total polymer powder, although much larger than the average molecular weights of the soluble polymer fraction, so that XO should not be regarded as an oligomer fraction. As shown later, the XO fraction is an atactic-rich polymer fraction, although it also contains certain amounts of isotactic chains of lower molecular weights. For this reason, Figure 11 shows that the Flory deconvolution does not lead to appropriate fitting of the experimental MWD obtained, which may also be observed through the small polydispersion indices evaluated experimentally for some samples. It is very probable that the proper understanding of the quality of the XO fraction has to involve both the kinetics of polymerization and the equilibrium/kinetics of polymer chain extraction by boiling xylene. Therefore, a detailed investigation of the extraction phenomena seems to be necessary if one is interested in understanding the nature of the XO fraction, which is certainly beyond the scope of this manuscript. In spite of that, Figure 12 shows that after the removal of the XO fraction, the MWD of the remaining insoluble polymer fraction cannot be fitted by the Flory deconvolution anymore, as the

Table VIII Deconvolution of the MWD of the XO Fractions

Experimental Tag	Order	θ_1	θ_2	α_1	PMn (g/gmol)	PMw (g/gmol)	PD
H0	2	1.83×10^{-4}	4.013×10^{-4}	0.355	139637	387097	2.772
H0	3	1.407×10^{-4}	8.924×10^{-4}	0.112	51989	150425	2.893
H1	9		6.348×10^{-4}	0.000	66185	128751	1.9453
H2	31		19.44×10^{-4}	0.000	21627	38965	1.802
H3	8	1.163×10^{-4}	13.07×10^{-4}	0.053	33793	99376	2.941
H4	32	1.266×10^{-4}	10.52×10^{-4}	0.145	45768	164390	3.592
H5	29		12.38×10^{-4}	0.000	33960	66032	1.944
H6	13	1.406×10^{-4}	16.21×10^{-4}	0.083	28056	97084	3.460
H8	11		24.07×10^{-4}	0.000	17469	30113	1.724

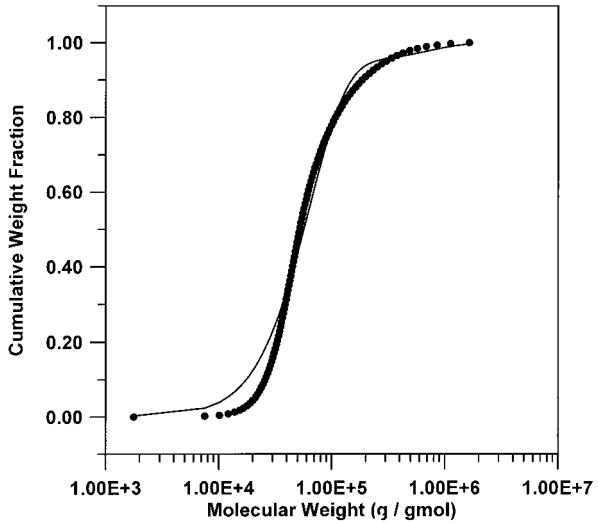

Figure 11 Deconvolution of the MWD of the XO fraction for polymerization H3–8, with the use of two site types. (●: experimental; ——: model.)

model consistently fails to describe the content of polymer chains at the lower chain size side of the graphic. This seems to support the fact that the XO fraction contains considerable amounts of isotactic chains of low molecular weight. Besides, a strong linear and statistically significant correlation (above 0.80) may be observed between the average molecular weights of the XO fraction and of the polymer powder, which also seems to support the assumption regarding the importance of extraction phenomena to describe the XO fraction and provides an empirical relationship to predict the quality of the XO material. For all these reasons, no additional attempts are made to describe the nature of the XO fraction based solely on the kinetics of polymerization.

Interpretation of Reaction Rate Curves

If reaction rates and/or polymer yields are measured, then it is possible to estimate the kinetic constants for chain growth and the relative amounts of catalyst sites as functions of reaction conditions. In order to do that, a kinetic mechanism is needed. The same mechanism described before, containing the usual activation, propagation, transfer, and catalyst decay steps, are used to interpret the experimental data. However, as pointed out before, more complex mechanisms may be used for this purpose. The numerical problem may then increase considerably, without any guarantee that improved performance of the process simulator will be obtained. However, if more complex mechanisms are to be used, the kinetic constants evaluated here may be used as initial guesses for additional parameter estimation.

Mathematical Modeling

The partial site activities α_j, $j = 1. . .N$, describe the mass fraction of polymer produced at site j. Therefore, α_j may be described as

$$\alpha_j = \frac{Kp_j\varphi_j[M][Cat]}{\sum_{i=1}^{N} Kp_i\varphi_i[M][Cat]} = \frac{Kp_j\varphi_j}{\sum_{i=1}^{N} Kp_i\varphi_i} \qquad (17)$$

where φ_j are the fractions of site j in the overall catalyst (or active species) mixture. Equation (17) shows very clearly that Kp_j and φ_j cannot be estimated simultaneously from GPC deconvolution, as these parameters are always multiplying each other. Therefore, *ad hoc* solutions must be proposed for estimation of catalyst site activities. A first approach may be assuming that catalyst site fractions or catalyst activities are the same for all sites. For Ziegler–Natta polymerizations it is generically believed that catalyst sites differ mostly because of the MWD of the polymer produced and not because of the amount of polymer produced in individual sites.[36] In this case,

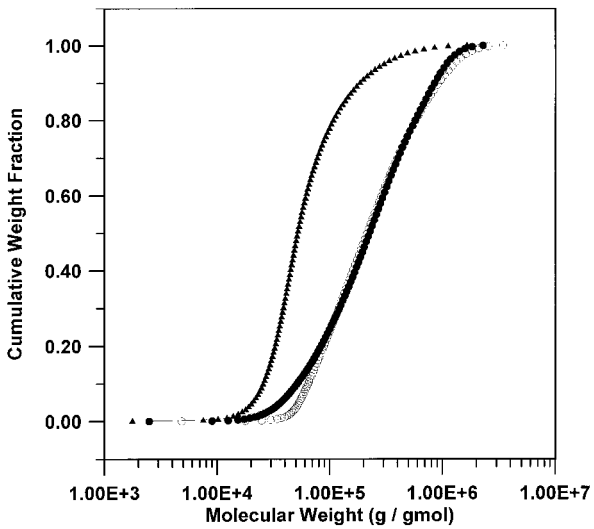

Figure 12 Comparison among the MWD of different polymer fractions for polymerization H3–8, with the use of two site types. (●: polymer powder; ▲ - XO fraction; ○: insoluble fraction; ——: model.)

$$\alpha_j = \frac{Kp_j}{\sum_{i=1}^{N} Kp_i} \quad \text{or} \quad \alpha_j = \frac{\varphi_j}{\sum_{i=1}^{N} \varphi_i} \tag{18}$$

A second approach might be assuming that the catalyst site fractions are known, in accordance to independent experimental investigations based on radio tagging, performed to unveil the intrinsic nature of the catalyst structure.[37] From a practical point of view, the best approach is the second one, as the first approach obliges the experimenter to model the catalyst synthesis, because variations of catalyst site fractions cannot be explained based solely on kinetic data. From a parameter estimation point of view, both approaches are equally adequate, if interpretation regarding the physical meaning of final parameter estimates is not required. In this work, the second approach is the one used. Catalyst site fractions are assumed to be of order $\varphi_j = 1.0 \times 10^{-3}$, as suggested in the literature for similar catalysts.[10,35]

Assuming that the original catalyst is a mixture of different catalyst sites, which must be activated before polymerization and that are subject to catalyst decay, then it is possible to write

$$\frac{dCat_j^0}{dt} = -Kr_j Cat_j^0 \tag{19}$$

$$Cat_j^0 = Cat_j^0(0)\exp(-Kr_j t) \tag{20}$$

$$\frac{dCat_j}{dt} = Kr_j Cat_j^0 - Kd_j Cat_j \tag{21}$$

$$Cat_j = \frac{Kr_j}{Kd_j - Kr_j} [\exp(-Kr_j t) - \exp(-Kd_j t)] Cat_j^0(0) \tag{22}$$

$$R_{\text{Pol}} = \sum_{j=1}^{N} Kp_j [M][Cat_j] = \sum_{j=1}^{N} A_j [\exp(-Kr_j t) - \exp(-Kd_j t)] \tag{23}$$

where Cat_j is the total mass of active catalyst site j, Cat_j^0 is the total mass of potential catalyst site j, t is time, Kr_j, and Kd_j are the kinetic constants for activation and decay of catalyst site j, R_{Pol} is the rate of polymerization, and A_j is a parameter lump, defined as

$$A_j = Kp_j \varphi_j^0 \frac{Kr_j}{(Kd_j - Kr_j)} [M][Cat] \tag{24}$$

It must be pointed out that $3N$ different parameters must be evaluated for each rate curve analyzed, unless additional simplifying assumptions may be introduced. For instance, if kinetic constants for activation and decay are similar for all catalyst site types, then eqs. (23) and (24) become much simpler:

$$R_{\text{Pol}} = \sum_{j=1}^{N} Kp_j [M][Cat_j] = A[\exp(-Krt) - \exp(-Kdt)] \tag{25}$$

$$A = \left(\sum_{j=1}^{N} Kp_j \varphi_j^0 \right) \frac{Kr}{(Kd - Kr)} [M][Cat] \tag{26}$$

where only three parameters must be estimated for each individual rate curve. One must observe that the parameters Kr_j, Kd_j, and A_j depend on the polymerization conditions and must be modeled afterward. For instance, hydrogen is believed to increase the rates of both catalyst activation and catalyst decay.[14] Besides, kinetic parameters certainly depend on reaction temperature. Therefore, standard correlation analysis must be performed for the estimated kinetic parameters to investigate whether polymerization conditions influence parameter estimates, to select the operation conditions for kinetic modeling and to allow the evaluation of activation energies for individual kinetic constants. But as kinetic constants must be provided for each catalyst site type, then it is interesting to combine eqs. (17) and (23) as

$$\alpha_j(t) = \frac{Kp_j \varphi_j^0 \frac{Kr_j}{(Kd_j - Kr_j)} [M][Cat] \times [\exp(-Kr_j t) - \exp(-Kd_j t)]}{\sum_{j=1}^{N} A_j [\exp(-Kr_j t) - \exp(-Kd_j t)]} \tag{27}$$

which must be averaged along the polymerization time to provide the experimental α_j values of the GPC deconvolution as

$$\alpha_j = \frac{Kp_j\varphi_j^0 \dfrac{Kr_j}{(Kd_j - Kr_j)}[M][Cat]\left[\dfrac{1-\exp(-Kr_jt)}{Kr_j} - \dfrac{1-\exp(-Kd_jt)}{Kd_j}\right]}{\sum_{j=1}^{N} A_j\left[\dfrac{1-\exp(-Kr_jt)}{Kr_j} - \dfrac{1-\exp(-Kd_jt)}{Kd_j}\right]} \tag{28}$$

However, if activation and decay properties of catalyst site types are similar, then it is possible to write

$$\alpha_j = \frac{Kp_j\varphi_j^0 \dfrac{Kr}{(Kd - Kr)}[M][Cat]}{A} \tag{29}$$

$$Kp_j\varphi_j^0 = \frac{\alpha_j A(Kd - Kr)}{[M][Cat]Kr} \tag{30}$$

Equations (27)–(30) show that GPC and rate data may be combined to provide the kinetic propagation constants for individual catalyst site types.

In this work, the interpretation of the rate curves comprises the following steps:

1. Estimation of parameters Kr_j, Kd_j, and A_j for catalyst sites, for increasing values of N. The iterative procedure is halted when the kinetic parameters obtained are not statistically significant or when the correlation coefficient between experimental and simulated results does not increase more than a few percents.
2. Combination of rate parameters with GPC deconvolution results to provide the kinetic constants for propagation of the individual catalyst site types.
3. Performance of standard correlation analysis between model parameters and reactor operation conditions to allow the selection of reaction conditions that cause variation of model parameters.
4. Modeling of kinetic parameters and computation of activation energies.

This mathematical procedure was implemented in FORTRAN for automatic interpretation of the experimental rate data, using a standard library of maximum likelihood parameter estimation routines.[33]

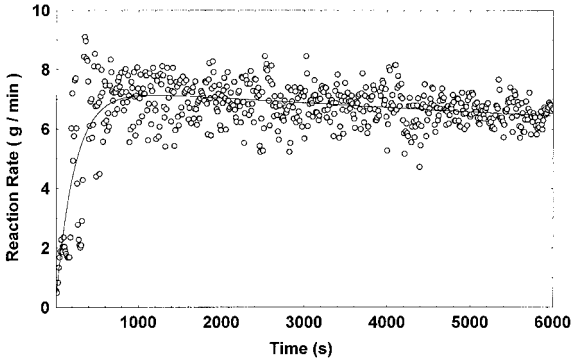

Figure 13 Polymerization rate profile for polymerization H6-13, assuming similar activation and deactivation constants for all catalyst sites. (○: - experiment; ——- model.)

Data Analysis

Figure 13 shows a typical polymerization rate profile obtained for the catalyst under investigation. Results indicate the existence of a very short activation period (5–10 min) and very small rates of catalyst decay, as polymerization rate decreases very slowly along the batch. This means that Kr_j are expected to be large and that Kd_j are expected to be very small. Besides, as Figure 13 shows results obtained in the absence of hydrogen, it is clear that fast activation and some degree of deactivation must be expected in all experimental conditions and do not depend exclusively on the addition of hydrogen to the reaction environment. As shown in Figure 13, no more than a single site is needed to reproduce rate data within the experimental accuracy in all experiments analyzed. This is an indication that eq. (25) is able to fit experimental results very well, and that it is reasonable to assume that activation and deactivation constants are similar for all catalyst sites. The whole set of parameter estimates obtained is shown in Table IX.

When correlation between Kr and the remaining variables are computed, very small correlation coefficients are obtained, which reflects the fact that Kr values are too big to be computed with accuracy with the experimental apparatus used in this study. From a practical point of view, though, this is not of much importance because Kr is so large that Kr uncertainties do not prejudice model predictions. It may be said that catalyst activation is almost instantaneous in the case analyzed. Modeling efforts are improved when Kr values that are larger than 60 h^{-1} are discarded, as activation would be finished in a couple of

Table IX Parameter Estimates Obtained from Reaction Rate Profiles

Experimental Tag	Order	A (g/min)	Kr (h^{-1})	Kd (h^{-1})
H0	2	2.3788	14.7027	0.2132
H0	3	2.7486	9.6932	0.2184
H0	4	3.5102	11.2810	0.3680
H0	5	3.5254	16.4248	0.3068
H1	6	0.9863	312.7781	0
H1	9	1.0756	354.3915	0.0247
H2	31	5.3155	31.5919	0.2887
H2	59	5.4763	57.4518	0.2322
H3	8	3.3667	19.2631	0.2773
H3	10	3.4815	30.1592	0.2549
H4	32	1.6484	20.8018	0.0776
H4	56	1.7525	37.2524	0.0762
H5	29	3.1811	43.1751	0.1571
H5	58	3.4588	44.5284	0.1009
H6	13	7.3669	16.0569	0.0813
H7	57	1.6712	25.4207	0.6394
H7	60	1.8972	21.3532	0.6580
H8	11	2.1492	33.7598	0
H8	12	2.0304	14.7490	0
H9	34	3.5394	16.0090	0.0332
H9	35	2.9504	10.9468	0.0639
H9	55	2.6834	20.3690	0.0254
H10	36	2.9881	47.9844	0.0474
H11	38	4.3780	22.2033	0.2086
H12	39	4.0182	63.3507	0.1364

minutes in these cases and there would not be many data points available for fair estimation of Kr. In this case, a significant statistical correlation of 0.65 is shown to exist between Kr and the cocatalyst/catalyst ratio used during catalyst preparation, which seems to indicate that catalyst activation depends mostly on the preparation conditions and on intrinsic morphological properties of the catalyst powder. It is usually accepted that catalyst activation depends basically on the rate of catalyst fragmentation during the first moments of the polymerization,[38–40] which is a function of particle size distribution and pore size distribution of catalyst grains. (This fact can also be used as an explanation for the similar values of Kr found for all catalyst site types.) As shown in a previous study,[26] both particle size and pore size distributions change a lot when catalyst preparation conditions are changed. Therefore, the result obtained sounds very consistent. An empirical model for Kr is then formulated as

$$Kr = \exp\left(10.45 - \frac{2433}{T_K}\right)(A/T_1)^{3.50} \quad (31)$$

where Kr is given in h^{-1} and A/T_1 is given in molar basis. Figure 14 shows that results obtained may be regarded as good. Equation (31) indicates that catalyst activation is faster at high temperatures and when A/T_1 is larger. The effect of temperature upon activation is trivial, while the effect of A/T_1 upon the catalyst activation rates is believed to be due to the increase of particle porosity.[26] The A/T_1 ratio cannot be increased too much though; otherwise, the catalyst grain becomes too fragile and excessive amounts of fines are produced during polymerization.

Compared to Kr, modeling of Kd is much easier because there is a significant degree of correlation between Kd and P_H for the data sets analyzed (0.87), when the zeroes are removed from the data set. (Values of $Kd = 0.0\ h^{-1}$ were obtained for experiments with very low polymer yields and for short batch times. For these experiments, consistent evaluation of Kd was not possible because of the low decay and large noise level of the rate profiles.) The following equation can then be obtained:

$$Kd = \exp\left(13.17 - \frac{5300}{T_K}\right) + \exp\left(4.74 - \frac{2223}{T_K}\right)P_H \quad (32)$$

where Kd is given in h^{-1} and the remaining variables are defined in Table I. Simulation results obtained may be regarded as very good, as illustrated in Figure 15. Equation (32) shows that catalyst decay increases with temperature, as expected, and with the partial hydrogen pressure, as well documented in the open literature.[14] It is interesting to observe that the decay constant

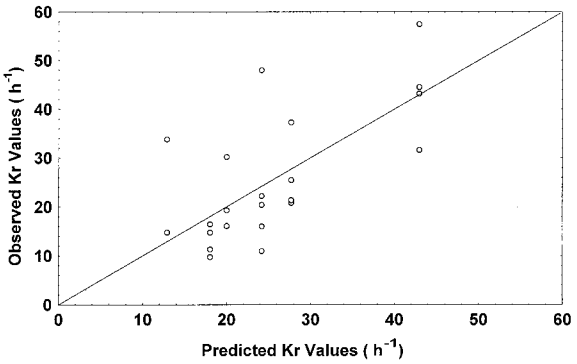

Figure 14 Observed and predicted activation rate constants for catalyst sites.

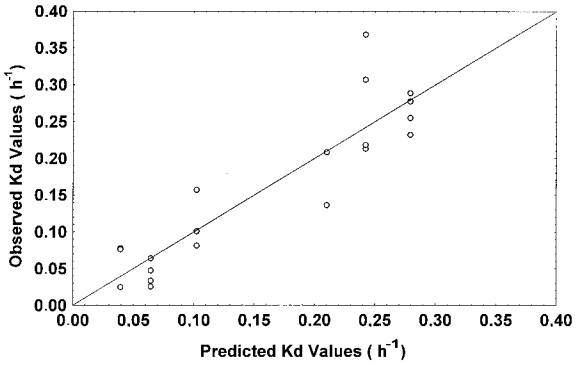

Figure 15 Observed and predicted decay rate constants for catalyst sites.

increases from 0.064 to 0.209 h^{-1} as P_H changes from 0 to 1 Kgf/$cm^2 \cdot$ g, which shows that hydrogen exerts an enormous influence upon catalyst stability. Alternative model formulations do not lead to any significant improvement of model predictions and were discarded.

As in the previous cases, standard correlation analysis was carried out for the propagation constants of both sites. It is interesting to observe that different results were obtained for each kinetic constant. For the propagation constant of the first site, important correlation was detected only for temperature. The Arrhenius form obtained for the kinetic constant is shown in eq. (33). Figure 16 illustrates the adequacy of the fit. There is some spread of data that cannot be removed with alternative formulations of the empirical model proposed. In spite of that, a correlation of 0.85 is obtained between experimental and simulation results of $Kp_1\varphi_1^0$.

$$Kp_1\varphi_1^0 = \exp\left(12.04 - \frac{6336}{T_K}\right) \qquad (33)$$

where $Kp_1\varphi_1^0$ is given in (g/min)/(Kgf/cm^2)/(mgTi/L).

For the second site, important correlations are detected for temperature and hydrogen partial pressure, which indicates that catalyst activity depends on the hydrogen concentration. Equation (34) shows the empirical fit obtained, while Figure 17 shows the adequacy of the model fit. Results may be regarded as very good and correlation between experimental and simulation results of $Kp_2\varphi_2^0$ are around 0.95.

$$Kp_2\varphi_2^0 = \exp\left(25.44 - \frac{11244}{T_K}\right) + \exp\left(6.51 - \frac{4627}{T_K}\right)P_H \qquad (34)$$

where $Kp_2\varphi_2^0$ is given in (g/min)/(Kgf/cm^2)/(mgTi/L).

It is well known that hydrogen exerts an important role for catalyst activation of propylene polymerizations[14] and this is explained nowadays in terms of multiple insertion polymerization mechanisms.[9] The intriguing fact here is that the catalyst sites responsible for production of the lower molecular weight fractions are the ones affected by hydrogen more strongly. As shown in the Appendix, the opposite behavior is normally expected with usual multiple insertion mechanisms, as the increase of the hydrogen concentration tends to release the sterically hindered catalyst sites for polymerization. Therefore, one might wonder whether some sort of chemical site activation, as proposed in many published works,[14] might also be responsible for the increase of catalyst activity observed or whether catalyst site

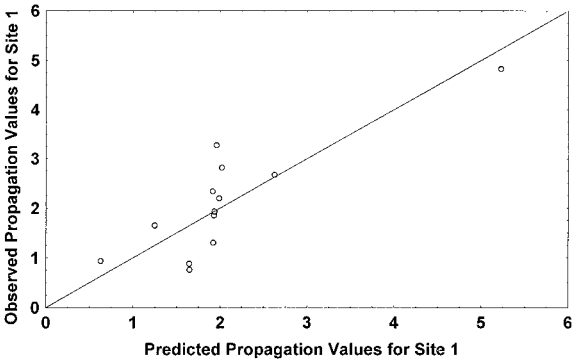

Figure 16 Observed and predicted propagation constants ($Kp_1\varphi_i^0$) for catalyst site 1 [in (g/min)/(Kgf/cm^2)/(mgTi/L)].

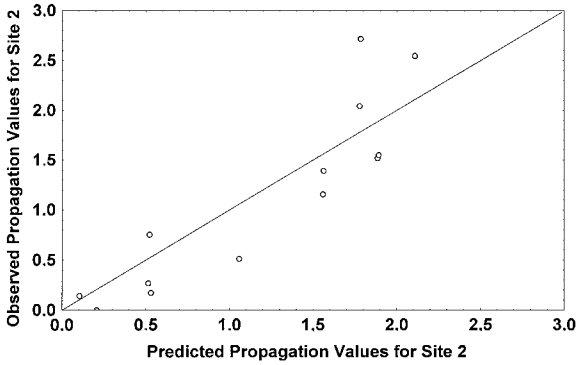

Figure 17 Observed and predicted propagation constants ($Kp_2\varphi_2^0$) for catalyst site 2 [in (g/min)/(Kgf/cm^2)/(mgTi/L)].

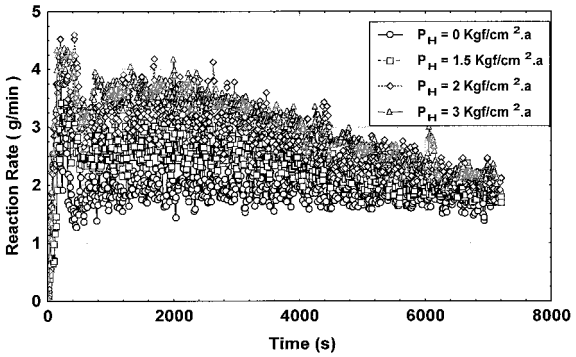

Figure 18 Polymerization rate profiles for different hydrogen concentrations.

type 1 might not be subject to stereochemical effects, that would only be observable for the site type 2. In this case, the catalyst would be well described by three different catalyst sites: catalyst site type 1 and the two stereo configurations of catalyst site type 2.

It must be noticed that at temperatures of 60°C, the activities of sites 1 and 2 change from 9.238 and 2.422 $\times$ 10^{-4} to 9.238 and 8.628 $\times$ 10^{-4}, respectively, as P_H changes from 0 to 1 Kgf/cm^2 · g. This represents an increase of catalyst activity of more than 50% in the presence of hydrogen, although leading to significant reduction of the weight average molecular weight, given the significant increase of the production of lower molecular weight polymer fractions. Unfortunately, detailed modeling of the hydrogen effect cannot be performed with two-level experimental designs. Due to the importance of the hydrogen effect observed, additional experiments were carried out with varying values of P_H, as described previously. Results are presented in the following section.

Additional Results Regarding the Hydrogen Effects

Experimental runs for increasing values of P_H were carried out for the standard experimental conditions (Tag H0 in Table I) and are shown in Table IV. The values of P_H used were equal to 0, 1.5,[2] and 3 Kgf/cm^2 · a, due to experimental constraints. Experiments were replicated and results obtained were very similar in all cases. Figure 18 shows how hydrogen partial pressure influences the final catalyst activity at 65°C. It can be seen graphically that both catalyst activity and catalyst decay increase with the increase of the hydrogen concentration. The kinetic constants obtained for each case are presented in Table 10. Figures 19 and 20 show how the kinetic constants change when P_H increases. Significant nonlinear effects are observed for *Kp* in the range analyzed, which agrees with the multiple insertion propagation mechanism (see Appendix), but can also be explained in terms of equilibrium kinetics. Both assumptions lead to very similar functional forms. For instance, assuming that certain catalyst sites are activated by hydrogen reversibly, as

$$Cat_j^{\mathrm{Pot}} + H_2 \underset{K_2}{\overset{K_1}{\rightleftharpoons}} Cat_j \tag{35}$$

then it is possible to write at equilibrium conditions

$$Cat_j = \frac{P_H}{K^{eq} + P_H}\,\varphi_j Cat_{Cat} \tag{36}$$

where K^{eq} is the ratio between K_2 and K_1. Figures 19 and 20 shows that eq. (36) provides excellent fits of observed experimental values of *Kp* and *Kd*. For *Kp*, eq. (36) becomes

$$Kp = 1.644 \times 10^{-3} + 1.438 \times 10^{-3}\,\frac{P_H}{1.216 + P_H} \tag{37}$$

which shows that hydrogen effects are important for relatively low values of P_H (below 3 Kgf/cm^2 · a) and that catalyst activation by hydrogen represents almost 50% of the maximum catalyst activity. Results obtained agree very well with re-

Table X Parameter Estimates Obtained from Reaction Rate Profiles for Varying Hydrogen Concentrations

P_H (Kgf/cm^2)	*Kd* (h^{-1})	*Kr* (h^{-1})	*Kp* (g/min)/(Kg f/cm^2)/(mg Ti/L)
0	0.0650	102.2720	0.0016
0	0.0475	65.4605	0.0017
1.5	0.2200	30.2013	0.0024
1.5	0.2413	32.0823	0.0024
2	0.2967	50.9347	0.0027
2	0.2657	43.8738	0.0025
2	0.2586	45.9801	0.0026
3	0.3109	31.2973	0.0026
3	0.3124	39.7477	0.0027

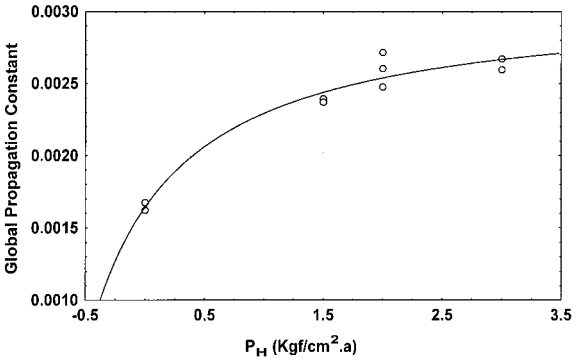

Figure 19 Global propagation constant as a function of hydrogen concentration. [*Kp* is given in (g/min)/(Kgf/cm^2)/(mgTi/L)].

sults presented in the previous section, for broader temperature and narrower hydrogen concentration ranges. For *Kd*, eq. (36) becomes

$$Kd = 0.056 + 0.456 \frac{P_H}{2.30 + P_H} \qquad (38)$$

which shows that hydrogen influence upon catalyst decay may be even more important than in the previous case, as catalyst deactivation induced by hydrogen may represent as much as 90% of the maximum catalyst deactivation rate possible. Besides, eq. (38) also shows that nonlinear effects are much less important to describe variations of the decay rate constant in the range of interest than observed previously for *Kp*.

Remarks Regarding Cocatalyst Effects

According to eq. (16), the cocatalyst may play an important role as a chain transfer agent during polymerization, especially when the partial hydrogen pressure is high and the relative amount of polymer produced at catalyst site 2 increases. However, this is not supported by actual operation data obtained at the plant site, which shows that the increase of the cocatalyst feed rates affects neither the catalyst activity nor the polymer average molecular weight at usual operation conditions. According to plant data, the increase of cocatalyst feed rates causes no significant effect upon plant operation, except the reduction of the XO polymer fractions when these values are too high, as shown in eq. (4). Therefore, at the plant site the cocatalyst is used mostly to control XO (although it is certain that polymerization conditions may change a lot if the cocatalyst concentration is allowed to fluctuate beyond the experimental range analyzed[21–23]). However, at plant site the catalyst feed solution is prepared and aged in feed tanks for approximately 1 h, due to production constraints (it must be guaranteed that feed tanks will never be empty!). Catalyst aging is known to cause variations of catalyst behavior, as catalyst site preparation depends fundamentally on a very complex set of reaction steps between the titanium and aluminum species.[11,41]

In order to investigate the influence of catalyst aging upon the final catalyst performance, polymerizations were carried out at the standard experimental conditions (Tag H0 in Table I), using two different catalyst feeds. The first one was the original catalyst feed described in Catalyst Preparation in the Experimental section of this article. The second one was prepared through aging of the original catalyst feed for 1 h inside the reactor vessel, with a solution containing 70% of the total cocatalyst feed and 100% of the diluent used for the polymerization batch. Results obtained are displayed in Figures 21 and 22. Figure 21 shows that reaction rates are slightly higher for the aged catalyst and that significant improvement of catalyst stability can be observed after catalyst aging. Figure 22 shows that molecular weight distribution is displaced to higher molecular weights and becomes broader after aging.

The relative decrease of the low molecular weight polymer fraction after aging probably explains why average molecular weights are not sensitive to changes of the cocatalyst concentration at the plant site. Besides, as catalyst sites that produce larger molecular weights also present higher activity, it sounds natural that the increase of average molecular weight and catalyst

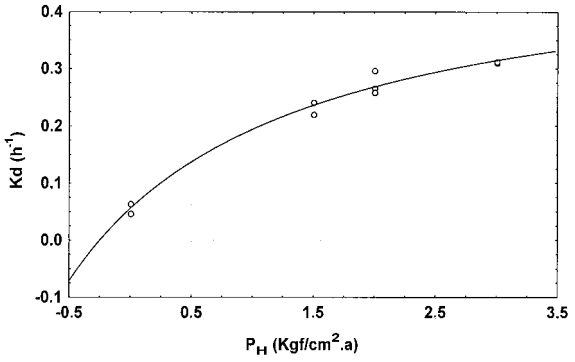

Figure 20 Catalyst decay rate constant as a function of hydrogen concentration.

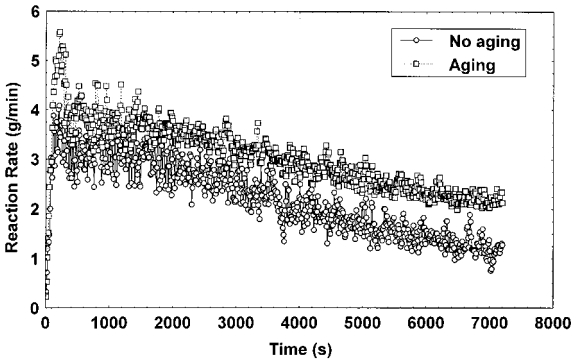

Figure 21 Polymerization rate profiles for catalysts submitted to different aging conditions.

activity occur simultaneously. This can also explain why catalyst activity is less sensitive to fluctuations of the hydrogen concentration at the plant site. It may be wondered then that significant catalyst stabilization may occur during the aging step, with reduction of the relative concentration of catalyst sites that lead to production of polymer with lower molecular weights. However, it must be pointed out that previous studies[11,41] indicate that aging generally exerts a negative effect upon catalyst activity, different from the experimental results obtained in this study (which were confirmed through replication).

It is not intended here to study the catalyst aging step in detail, but it is important to say that the experimental procedure implemented here was able to detect that catalyst aging may be important for a description of final catalyst performance. It is also important to observe that if chain transfer to cocatalyst is neglected, then the remaining kinetic constants presented are able to describe fairly well the polymer product obtained at plant site in Polibrasil Resinas SA, Camaçari—BA, Brazil.

Interpretation of NMR Spectra

If NMR spectra of polymer samples are available, then it is possible to observe the detailed internal structure of polymer chains, allowing a much better understanding of copolymer and stereochemical block formation. As observed in the previous cases, however, a kinetic model is needed to allow the proper kinetic interpretation of the NMR spectra. In a certain sense, NMR modeling is easier than traditional kinetic modeling, because NMR spectra depend mostly on chain growth steps, which occur much more frequently than the other reaction steps. For the sake of coherence, the same sort of kinetic model used before is used again for NMR kinetic interpretation. As shown in the literature,[34] the model can be changed to accommodate more complex kinetic mechanisms.

Mathematical Modeling

The most important characteristic of the internal structure of polypropylene chains is the stereoregular distribution of the methyl groups along the polymer backbone (tacticity). Methyl groups may be inserted along the same side (isotactic m-insertion) or along the opposite sides (syndiotactic r-insertion) of the backbone during polymerization. When a block sequence containing N_b (number of blocks for NMR analysis) molecules is analyzed, the number of possible arrangements of the methyl groups is

$$N_{\mathrm{Arr}} = 2^{(N_b-1)} \tag{39}$$

However, certain pairs of arrangements are mirrored copies of each other, which means that they actually represent a single chemical structure. For instance, the sequence mmmr is identical to the sequence rmmm, depending only on the direction selected to count the branching sequence along the polymer backbone. The total number of different stereo-blocks formed when N_b molecules are analyzed is therefore obtained by subtracting the number of possible mirrored copies from the total number of possible arrangements, as

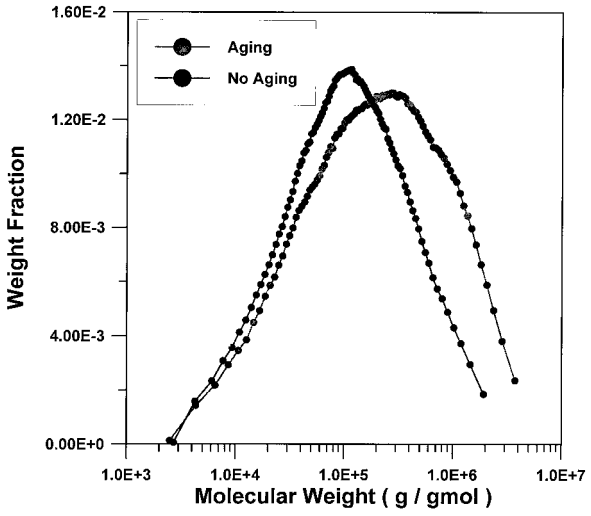

Figure 22 MWD of polymer powders obtained with catalysts submitted to different aging conditions.

$$N_{\text{blocks}} = \frac{2^{(N_b-2)}}{2^{[\text{INT}(N_b-1)/2]}}\,[2^{[\text{INT}(N_b-1)/2]}+1], \qquad N_b \geq 2 \quad (40)$$

where INT(·) is the function that keeps the integer part of a real number. If mass balances are now written for each individual stereo-regular block, then it is possible to compute the concentrations of N-ads (the sequences of N_b molecules that form the blocks) during polymerization.[34] Assuming that stereo-block formation is controlled by propagation and that the ultimate model can be used to describe the formation of stereo-blocks, then the following insertion steps may be used to describe the reaction mechanism:

$$\begin{cases} S + M \xrightarrow{K_{SS}} S \\ S + M \xrightarrow{K_{SR}} R \\ R + M \xrightarrow{K_{RS}} S \\ R + M \xrightarrow{K_{RR}} R \end{cases} \quad (41)$$

where S and R represent two distinct stereo-configurations of the active site (determined by the position of the methyl group). It is not intended to discuss here the detailed stereo-chemistry of Ziegler–Natta catalysts, because the literature about the subject is vast and because each catalyst may present individual characteristics that are not shared by other catalysts.[34] It is assumed here that isotactic insertions preserve the stereo-chemistry of the active site, while syndiotactic insertions change the stereo-chemistry of the active site. (This assumption is not of fundamental importance and other catalysts can be analyzed as presented below with simple redefinition of kinetic constants.[34]) Assuming that polymerization conditions remain constant and that the quasi steady state assumption is valid for active species, it is possible to write

$$[R_j] = \frac{K_{SR}}{K_{SR}+K_{RS}}\,\varphi_j[Cat] \quad (42)$$

$$[S_j] = \frac{K_{RS}}{K_{SR}+K_{RS}}\,\varphi_j[Cat] \quad (43)$$

(R_j and S_j are the sterero-block R and S configurations, respectively), which can be renormalized as

$$r_j = \frac{\Pi_{SR}}{\Pi_{SR}+\Pi_{RS}} \quad (44)$$

$$s_j = \frac{\Pi_{RS}}{\Pi_{SR}+\Pi_{RS}} \quad (45)$$

where r_j and s_j are the fractions of sites with the R and S configurations respectively, and Π_{ij} are the insertion probabilities, defined as

$$\Pi_{ij} = \frac{K_{ij}}{Kp}, \quad i,j = R, S \quad (46)$$

It is implicitly assumed here that

$$K_{SS} + K_{SR} = K_{RS} + K_{RR} = Kp \quad (47)$$

$$K_{SS} + K_{SR} = K_{RS} + K_{RR} = Kp \quad (48)$$

If eq. (47) is not satisfied, then a multistep propagation mechanisms must be used, as presented in the Appendix. Equation (47) says that the particular stereo-configuration of the methyl group does not affect propagation. (As far as iso/syndio insertions are concerned, this may be a good assumption for most Ziegler–Natta catalysts. However, the story is completely different when head/tail insertions are analyzed.)

The NMR model can then be built as

$$B_k = \sum_{j=1}^{N} \alpha_j b_{kj} \quad (49)$$

where B_k is the molar fraction of stereo-block k at the final polymer, α_j is the mass fraction of polymer produced at site j, and b_{kj} is the molar fraction of the stereo-block k produced at site j.The b_{kj} is a function of the block size, of the block configuration, and of the kinetic constants. As far as the assumptions presented above are valid, the values of b_{kj} may be computed using traditional statistical arguments, which say that

$$\Pi(A, B) = \Pi_A \Pi_{B/A} \quad (50)$$

Put into words, eq. (50) estates that the probability of observing occurrences A and B in a row is the probability for occurrence of event A times the

Table XI NMR Deconvolution Models for Pentad Distributions

k	Tacticity	Kinetic	Ultimate Model	Terminal Chain Model
1	mmmm	RRRRR SSSSS	$r\Pi_{RR}^4 + s\Pi_{SS}^4$	Π_{ISO}^4
2	mmmr	RRRRS SSSSR RSSSS SRRRR	$r(\Pi_{RR}^3\Pi_{RS} + \Pi_{RS}\Pi_{SS}^3) + s(\Pi_{SS}^3\Pi_{SR} + \Pi_{SR}\Pi_{RR}^3)$	$2\Pi_{ISO}^3(1 - \Pi_{ISO})$
3	mmrm	RRRSS SSSRR RRSSS SSRRR	$r(\Pi_{RR}^2\Pi_{RS}\Pi_{SS} + \Pi_{RR}\Pi_{RS}\Pi_{SS}^2) + s(\Pi_{SS}^2\Pi_{SR}\Pi_{RR} + \Pi_{SS}\Pi_{SR}\Pi_{RR}^2)$	$2\Pi_{ISO}^3(1 - \Pi_{ISO})$
4	mmrr	RRRSR SSSRS RSRRR SRSSS	$r(\Pi_{RR}^2\Pi_{RS}\Pi_{SR} + \Pi_{RS}\Pi_{SR}\Pi_{RR}^2) + s(\Pi_{SS}^2\Pi_{SR}\Pi_{RS} + \Pi_{SR}\Pi_{RS}\Pi_{SS}^2)$	$2\Pi_{ISO}^2(1 - \Pi_{ISO})^2$
5	mrmr	RRSSR SSRRS RSSRR SRRSS	$r\begin{pmatrix}\Pi_{RR}\Pi_{RS}\Pi_{SS}\Pi_{SR} + \\ \Pi_{RS}\Pi_{SS}\Pi_{SR}\Pi_{RR}\end{pmatrix} + s\begin{pmatrix}\Pi_{SS}\Pi_{SR}\Pi_{RR}\Pi_{RS} + \\ \Pi_{SR}\Pi_{RR}\Pi_{RS}\Pi_{SS}\end{pmatrix}$	$2\Pi_{ISO}^2(1 - \Pi_{ISO})^2$
6	rmmr	RSSSR SRRRS	$r\Pi_{RS}\Pi_{SS}^2\Pi_{SR} + s\Pi_{SR}\Pi_{RR}^2\Pi_{RS}$	$\Pi_{ISO}^2(1 - \Pi_{ISO})^2$
7	mrrm	RRSRR SSRSS	$r\Pi_{RR}^2\Pi_{RS}\Pi_{SR} + s\Pi_{SS}^2\Pi_{SR}\Pi_{RS}$	$\Pi_{ISO}^2(1 - \Pi_{ISO})^2$
8	mrrr	RRSRS SSRSR SRSRR RSRSS	$r(\Pi_{RR}\Pi_{RS}^2\Pi_{SR} + \Pi_{RS}^2\Pi_{SR}\Pi_{SS}) + s(\Pi_{SS}\Pi_{SR}^2\Pi_{RS} + \Pi_{SR}^2\Pi_{RS}\Pi_{RR})$	$2\Pi_{ISO}(1 - \Pi_{ISO})^2$
9	rmrr	RSSRS SRRSR SRSSR RSRRS	$r(\Pi_{RS}^2\Pi_{SS}\Pi_{SR} + \Pi_{RS}^2\Pi_{SR}\Pi_{RR}) + s(\Pi_{SR}^2\Pi_{RR}\Pi_{RS} + \Pi_{SR}^2\Pi_{RS}\Pi_{SS})$	$2\Pi_{ISO}(1 - \Pi_{ISO})^3$
10	rrrr	RSRSR SRSRS	$r\Pi_{RS}^2\Pi_{SR}^2 + s\Pi_{SR}^2\Pi_{RS}^2$	$(1 - \Pi_{ISO})^2$

probability of occurrence of B, given the fact that A has already occurred.

Let us assume, for instance, that pentads are being analyzed ($N_b = 5$). In this case, eq. (40) says that the number of different stereo-blocks is equal to 10, as shown in Table XI. As individual blocks may be initiated by either R or S and either from left to right or right to left, then all conditions must be taken into consideration as described by eq. (50), leading to the values of b_{kj} shown in Table XI. The model, in this case, depends on $3N - 1$ parameters (Π_{RRj}, Π_{SSj}, α_j). Π_{RRj} and Π_{SSj} are the degrees of isotacticity of the R and S stereo configurations of site j respectively.

If one observes that a maximum of 10 pentads are observed through the NMR spectra, it is easy to understand that the model has too many parameters. The problem, though, is that some pentads cannot be observed or are confounded with other NMR signals. Besides, even when pentads can be seen in the NMR spectra, sometimes the concentrations are so low that they are of the order of magnitude of the experimental error (believed to be within the range of a few percents). Therefore, it is very hard to estimate kinetic parameters from NMR spectra in practice. One possible solution is increasing the number of possible N-ads, using NMR instruments of larger power and resolution than the one used in this work (for instance, 544 decads—$N_b = 10$—may be shown to exist). However, if the degree of isotacticity is high (for instance, 0.98), as for most modern catalysts, then the molar fraction of isotactic decads is of order 0.82, while the remaining decad con-

centrations are lower than 0.017, which means that the estimation problem remains.

In order to reduce the number of parameters, it may be assumed that the degrees of isotacticity are the same and do not depend on the particular stereo configuration of the catalyst site. In this case, the monomer insertion is supposed to depend exclusively on the terminal chain configuration, so that

$$\Pi_{ISO} = \Pi_{SS} = \Pi_{RR} \tag{51}$$

The model then becomes much simpler, as shown in Table XI. The number of parameters is reduced to $2N - 1$, which is still too high for most practical reasons.

In this work, the NMR interpretation then comprises the following steps:

1. Assignment of N-ads and theoretical molar fraction distributions, based on the ultimate or terminal chain models.
2. Estimation of parameters Π_{RRj}, Π_{SSj}, and α_j (or Π_{ISO} and α_j) for catalyst sites, for increasing values of N. The iterative procedure is halted when the kinetic parameters obtained are not statistically significant or when the correlation coefficient between experimental and simulated results does not increase more than a few percents.
3. Performance of standard correlation analysis between model parameters and reactor operation conditions to allow the selection of reaction conditions that cause variation of model parameters.
4. Modeling of kinetic parameters and computation of activation energies.

From a practical point of view, α_j may be regarded to be known, as this parameter was estimated in the previous steps. Execution of step 2 of the algorithm shown above, however, is highly recommended for proper estimation of model parameters. It is also interesting to observe that all model parameters must be constrained between 0 and 1. To make estimation easier and avoid generation of unrealistic model parameters, it may be convenient to write model parameters as

$$\Pi = \frac{\exp(\lambda)}{1 + \exp(\lambda)} \tag{52}$$

where λ is a transformed model parameter and Π is the actual model parameter. This way, the inequality constraints are automatically satisfied and no constraint must be placed on λ.

Data Analysis

Figures 23, 24, and 25 show typical NMR spectra obtained for solubles, XO, and final polymer powder. As observed experimentally, the final pentad distribution obtained for samples of different experimental runs are extremely similar and vary within the range of experimental error ($\pm 2\%$), which seems to indicate that the internal microstructure of the polymer is not much sensitive to changes of the experimental conditions. Similar results have been obtained previously for other catalysts.[21–23] This makes modeling of stereo-block distribution much easier for this particular catalyst analyzed. Results obtained with the terminal chain model are illustrated in Figure 26. For solubles and XO, theoretical results were obtained assuming that two sites were present with

$$\begin{cases} \alpha_1 = 0.08, & \Pi^1_{ISO} = 0.96 \\ \alpha_2 = 0.92, & \Pi^1_{ISO} = 0.45 \end{cases}$$

while theoretical results for the final polymer powder were obtained assuming that a single site was present, with $\Pi_{ISO} = 0.95$.

The results obtained show that the soluble and XO fractions are constituted mostly of atactic polypropylene, although a small portion of highly isotactic material is also taking part of the mixture. As the molecular structure of both solubles and XO are very alike, it may be concluded that the main difference between these two fractions is the molecular weight distribution. Regarding the final polymer powder, no more than one single site could be detected, which means that material is relatively homogeneous at the stereo-block level and that both sites observed in the previous section produce material of relatively high degree of isotacticity. It may be concluded then that atactic catalyst sites are present at relatively low concentrations and that most of the atactic material is removed by the diluent during polymerization at normal conditions. Compared to more advanced catalysts, the degree of isotacticity of the Ziegler–Natta catalyst analyzed is relatively low, leading to average isotactic block sizes of 20 monomer units.

The terminal chain model fits NMR data very well, except for pentad rmmr, where a systematic negative deviation seems to occur. As results are not improved when the number of sites is in-

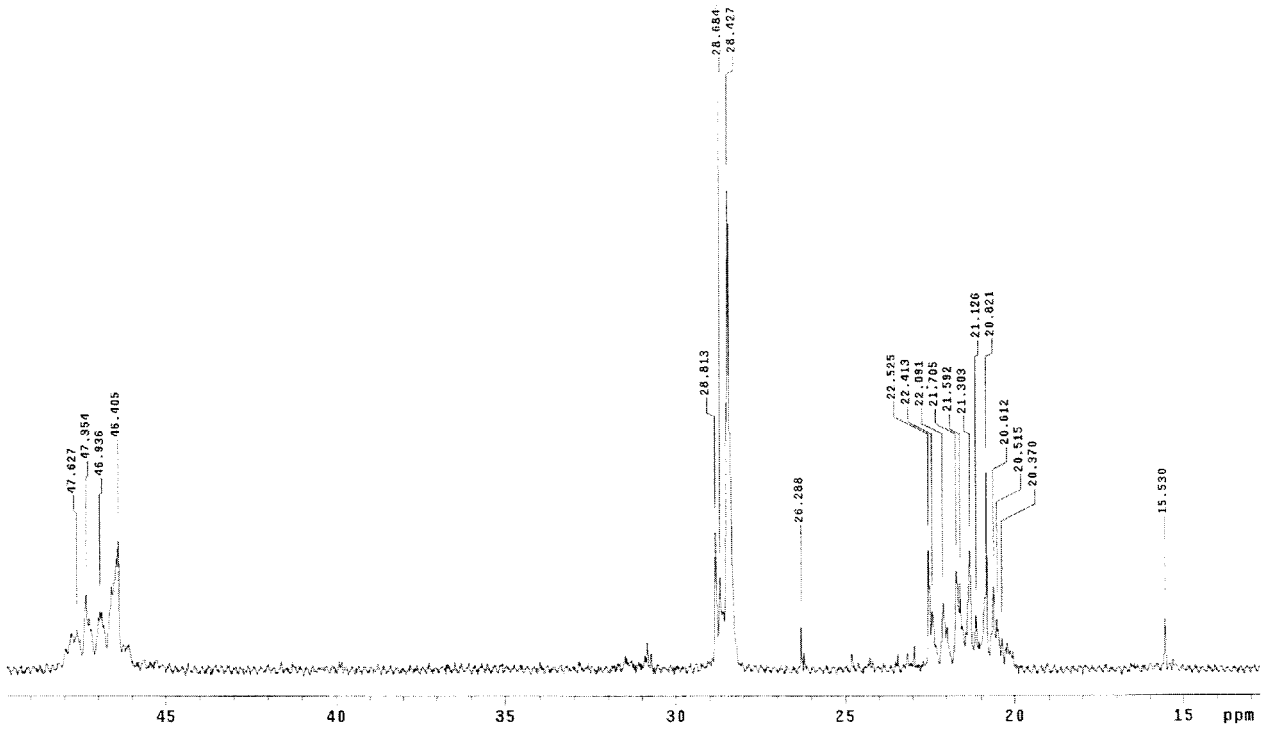

Figure 23 Typical NMR spectra of the soluble fraction. (Experimental run H4–32.)

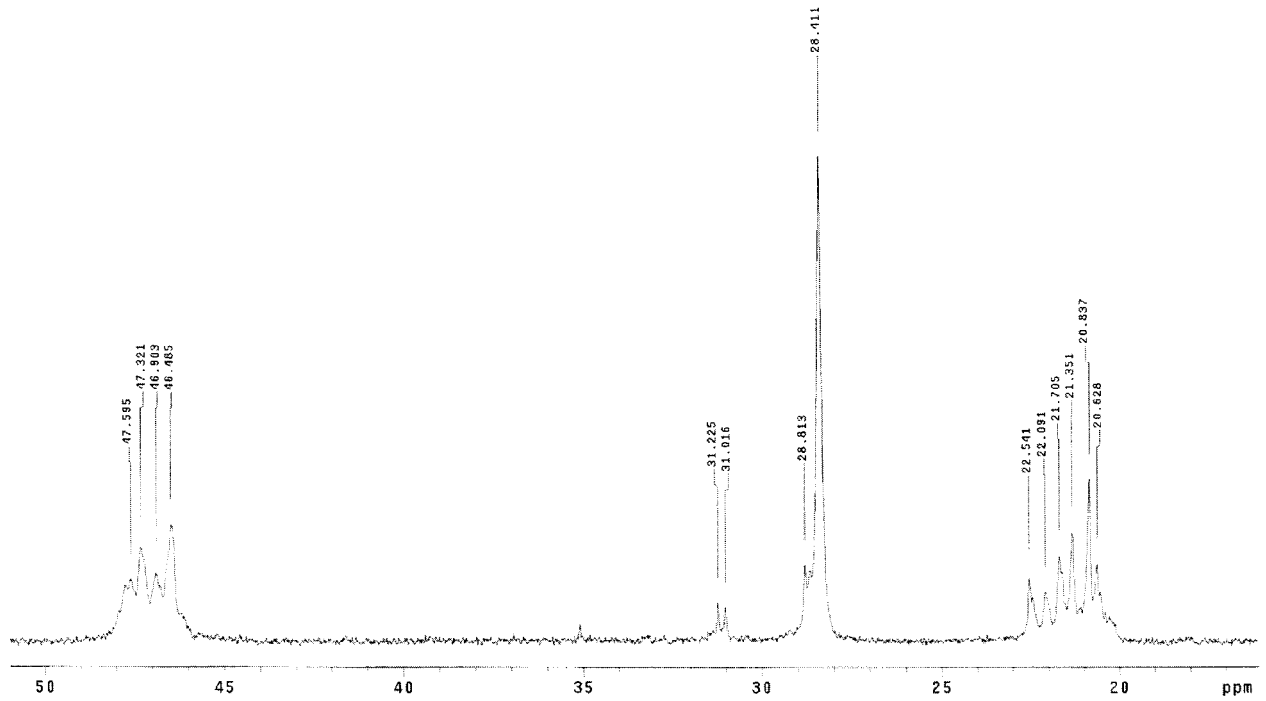

Figure 24 Typical NMR spectra of the XO fraction. (Experimental run H4–32.)

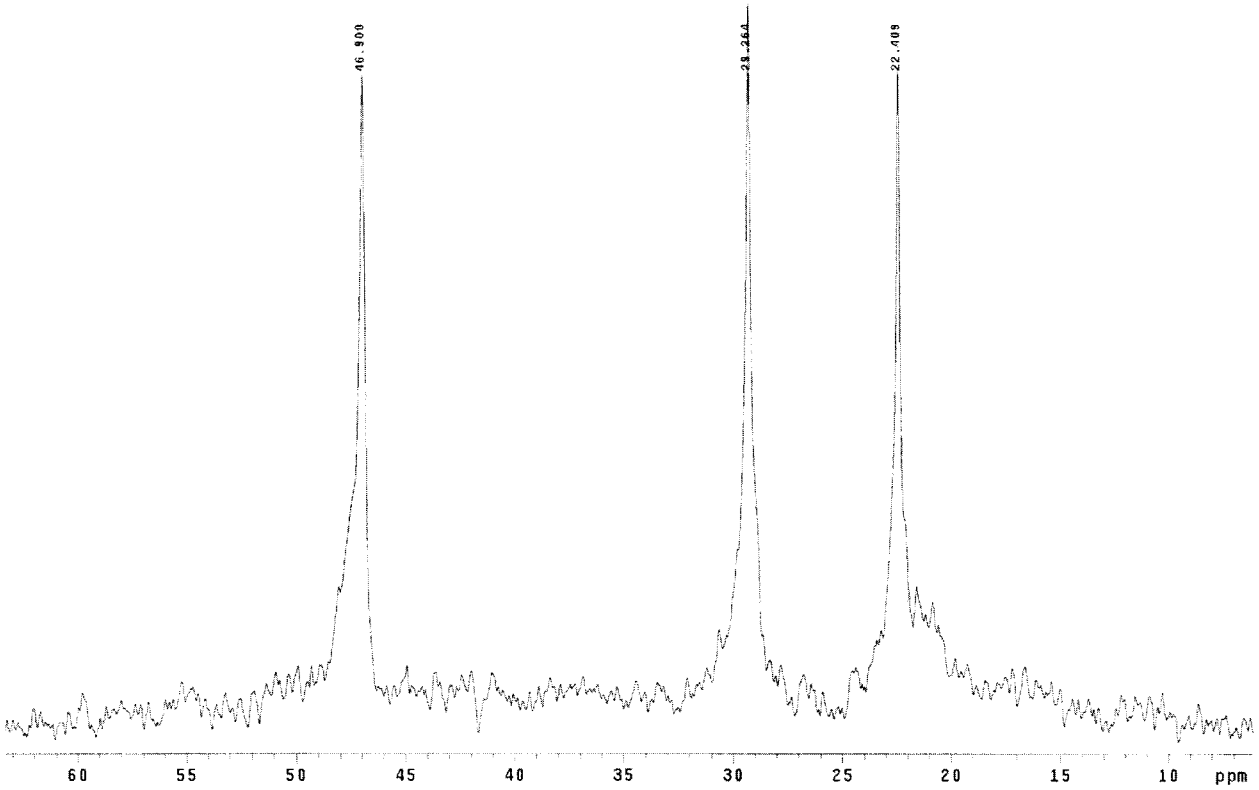

Figure 25 Typical NMR spectra of the polymer powder. (Experimental run H4–32.)

creased and given the lack of more precise data, no attempt was made to improve model predictions. Discussions about detailed fitting of NMR spectra may be found elsewhere.[42] For most practical reasons, results may be regarded as very good.

Final Remarks

Kinetic constants and activation energies obtained here are in good agreement with values presented by surveys in the literature.[10,35] Therefore, results obtained may be regarded as consistent. However, to the best of out knowledge, results presented here constitute the largest set of kinetic constants obtained for a single catalyst and specific polymerization conditions already presented in the literature, including characterization of number of catalyst site types and specific kinetic constants for each site type. It is common in the literature to present individual kinetic constants for atactic catalyst sites, based on polymer fractions obtained through solvent extraction. This is not done here because, as discussed before, thermodynamic phenomena probably play a major role for proper explanation of the amounts of solubles and XO fractions obtained through solvent extraction. For this reason, eqs.(3) and (4) are used for characterization of these particular polymer fractions in the process simulator.

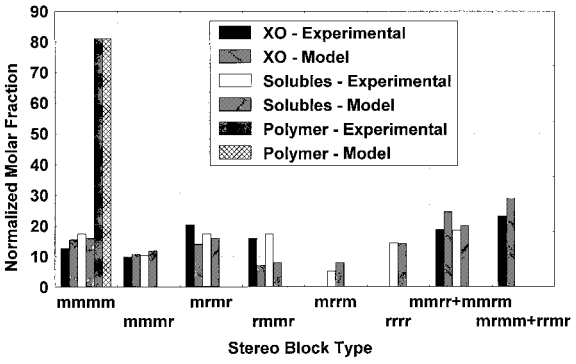

Figure 26 Pentad distribution for polymer samples, using the terminal chain model. (Experimental run H4–32.)

In order to validate the set of kinetic constants obtained here at actual process operation conditions, the kinetic data set was inserted into the simulator SIMULPOL 3.0[43] and used for simulation of a typical slurry propylene polymerization

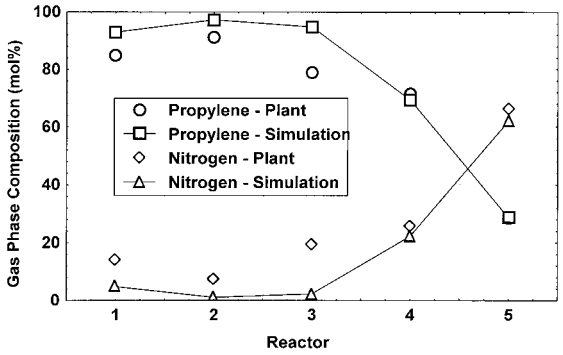

Figure 27 Gas composition profiles as measured at plant site and predicted through simulation.

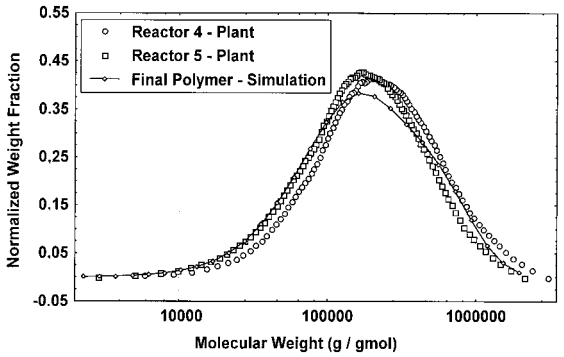

Figure 29 Molecular weight distribution obtained at plant site and predicted through simulation.

process. Details regarding the process configuration are presented elsewhere,[44] but it is important to say that the process comprises 5 stirred tank reactors in series and that reactants are added to the first 3 reactors of the train. Figure 27 shows the gas composition profiles for the major gas constituents: propylene and nitrogen. Results indicate that catalyst activity is predicted correctly. Figure 28 shows the melt flow index (MI) of the grades produced by Polibrasil Resinas SA and predictions obtained with the process simulator. Results may be regarded as excellent and indicate that chain transfer phenomena are predicted successfully. Finally, Figure 29 shows the molecular weight distribution for one polymer grade produced at plant site, as predicted by the simulator and measured experimentally. Results are fairly good and indicate the consistency of the multisite approach. Besides, the amounts of solubles and the XO of the polymer resin are predicted with precision within the experimental error. For instance, at typical operation conditions the experimental values obtained were equal to 1.92 and 4.73 respectively, while model predictions were equal to 1.97 and 4.77, respectively. Finally, the degree of isotacticity obtained through NMR analysis of the final polymer powder is equal to the isotacticity of the polymer powder obtained in the lab (0.95–82% of isotactic pentads), confirming that the degree of isotacticity is not sensitive to fluctuations of the process operation conditions within the ranges analyzed.

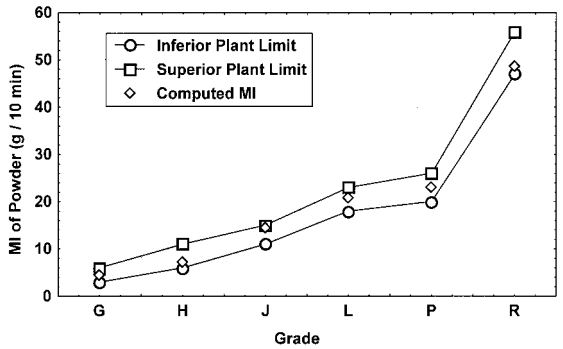

Figure 28 Melt flow index of polymer grades obtained at plant site and predicted through simulation.

Regarding the time needed for carrying out the whole kinetic data analysis, it may be said that it would take about six weeks (on a basis of 40 h of work per week) for an experienced engineer to go through the different steps of the method proposed. About 15 days would be needed for carrying out experiments. An additional 15 days would be needed to characterize the polymer samples properly. Finally, 15 more days would be needed for data analysis and model computations. It is assumed here that the experimental setup is ready and running, that polymer characterization is carried out in available computerized lab machines, and that model equations are implemented in a personal computer. Otherwise, additional time will be needed for proper data transferring between lab machines and the personal computer (which must not be neglected!) and for implementation of mathematical routines. Therefore, the method proposed here may certainly be incorporated as a daily routine for catalyst development and characterizations in the polyolefins business, especially because it allows the fast analysis through simulation of the impact of catalyst drop-in into actual polymerization processes. It must be emphasized that additional costs needed for catalyst kinetic characterization, as proposed here, are certainly negligible when

compared to the costs of catalyst and process development. As process *scale-up* may be carried out more efficiently if kinetic data are available and kinetic data may be regarded as part of the process technology, additional costs for kinetic characterization can certainly be recovered with huge profits during process development.

CONCLUSIONS

A method was presented for kinetic characterization of catalysts for olefin polymerizations, in order to allow the estimation of kinetic parameters for use in process simulators. The method allowed the successful characterization of conventional first-generation Ziegler–Natta catalysts for slurry propylene polymerizations with relatively few experiments. The total number of experiments performed was equal to 40, corresponding to 17 different experimental conditions, as replicates were carried out to assure the consistency of the experimental results. Eleven experimental conditions were used for main effect analysis, 5 additional experimental conditions were used for specific hydrogen studies and 1 additional experimental condition was used for analyzing the aging step. The experiments allowed the evaluation of the effects caused by 8 independent variables upon the final polymerization results. The method presented here relies on the availability of polymerization rate profiles, GPC chromatograms, and NMR spectra of polymer samples. As the number of proposed experiments is relatively small and the techniques used for polymer characterization are rather standard, the method can be implemented at plant site very easily and encourage the use of process simulators for actual process studies.

Results obtained show that the amounts of soluble and XO polymer fractions produced, often used for quality control routines at plant site, cannot be interpreted based solely on kinetic models, as thermodynamic effects seem to play an important role for proper description of these variables. Besides, it was shown that the main difference between samples of these fractions regards the molecular weight distribution, as both fractions are constituted mostly by atactic material. It was also shown that chain transfer to monomer controls the molecular weight distribution of the final polymer obtained with the catalyst analyzed, placing a bound upon the maximum weight average molecular weight that can be obtained at plant site around $8x10^5$ g/gmol. The method allowed the detection of important hydrogen and catalyst aging effects upon the catalyst activity, catalyst stability and molecular weight distribution of the polymer product. It was observed for this catalyst that the increase of the hydrogen concentration seems to exert a much more pronounced effect upon the catalyst activity of sites that produce material of low molecular weight than upon the chain transfer rate to hydrogen. Additionally, it was shown that the internal stereo-block configuration of polymer chains is not sensitive to changes of the polymerization conditions in the range analyzed, so that the catalyst performance at the stereo-block level is essentially constant.

The kinetic parameters estimated with the help of simple kinetic models were inserted into a process simulator and allowed the proper description of plant operation. Therefore, the consistent set of parameters presented here may be used as a benchmark for simulation studies of slurry propylene polymerizations and as initial guesses for development of more complex kinetic models.

APPENDIX

A very simple multiple insertion mechanism may be formulated as

$$\begin{cases} C_0 + M \xrightarrow{K_{pP}} P \\ C_0 + M \xrightarrow{K_{pQ}} Q \\ P + M \xrightarrow{k_{pP}} P \\ P + M \xrightarrow{k_{pQ}} Q \\ P + H_2 \xrightarrow{k_{tP}} C_0 + \text{Pol} \\ Q + H_2 \xrightarrow{k_{tQ}} C_0 + \text{Pol} \end{cases} \tag{A1}$$

where it is assumed that two distinct stereochemical forms are produced during polymerization.

The form P is active for polymerization, while form Q is inactive (or presents much lower polymerization activity). However, both forms can undergo chain transfer to hydrogen, allowing the production of new polymer chains. Assuming that the quasi steady state assumption is valid, then it is possible to write:

$$P = \frac{1}{k_{pQ}M + k_{tP}H_2} k_{pP}C_0M \quad \text{(A2)}$$

$$Q = \frac{1}{k_{tQ}H_2}\left[\frac{k_{pQ}M + k_{tP}H_2 + k_{pP}M}{k_{pQ}M + k_{tP}H_2}\right]k_{pQ}C_0M \quad \text{(A3)}$$

As

$$P + Q + C_0 = Cat \quad \text{(A4)}$$

Equations (A2)–(A4) can be solved for P, Q, and C_0, as functions of the total amount of catalyst available in the system. Then, the rate of polymerization at catalyst sites of type P can be computed as

$$R_{\text{pol}} \cong k_{pP}MP = \frac{k_{pP}MCat}{k_{tQ}} \frac{H_2}{H_2 + \dfrac{k_{pQ}M}{k_{tQ}}} \quad \text{(A5)}$$

which is similar to eq. (36) and shows that the activity of the polymerization as a whole and of the active sites in particular increase with the increase of the hydrogen concentration. This picture does not change when the form Q is also assumed to polymerize at rates different from zero.

The authors thank Polibrasil Resinas SA for supporting this project. The authors are also indebted to all engineers of Polibrasil for valuable discussions and sound advice. The authors also thank Prof. Maria Inês Bruno, from Instituto de Macromoléculas, Universidade Federal do Rio de Janeiro, for the NMR characterization of polymer samples.

REFERENCES

1. Moore, E. P., Jr.; Larson, G. A. In Polypropylene Handbook; Moore, E. P., Jr., Ed.; Hanser Publishers: Cincinatti, OH, 1996.
2. Zabisky, R. C. M.; Chan, W.-M.; Gloor, P. E.; Hamielec, A. E. Polymer 1992, 33, 2243–2262.
3. Soares, J. B. P.; Hamielec, A. E. Polym React Eng 1996, 4, 153–191.
4. Xie, T.; McAuley, K. B.; Hsu, J. C. C.; Bacon, D. W. Ind Eng Chem Res 1994, 33, 449–479.
5. Zacca, J. J.; Debling, J. A.; Ray, W. H. Chem Eng Sci 1996, 51, 4859–4886.
6. Nele, M.; Pinto, J. C. J Appl Polym Sci 2000, 77, 433–452.
7. Huang, J.; Rempel, G. L. Progr Polym Sci 1995, 20, 459–526.
8. Fink, G.; Fenzl, W.; Herfert, N.; Miller, T.; Jaber, I. In Catalytic Olefin Polymerization; Keii, T.; Soga, K., Eds.; 1989; pp 223–243,
9. Chadwick, J. C.; van Kessel, G. M. M.; Sudmeijer, O. Macromol Chem Phys 1995, 196, 1431–1437.
10. Zakharov, V. A.; Bukatov, G. D.; Ermakov, Y. I. Russ Chem Rev 1980, 49, 1097–1111.
11. Yoon, J.-S.; Ray, W. H. Ind Eng Chem Res 1987, 26, 415–422.
12. Li, J.; Tekie, Z.; Mohammad, A.; Morsi, B. I. Can J Chem Eng 1996, 74, 77–83. 13. McKenna, T. F.; Dupuy, J.; Spitz, R. J Appl Polym Sci 1997, 63, 315–322.
14. Alex Shaffer, W. K.; Ray, W. H. J Appl Polym Sci 1997, 65, 1053–1080.
15. Embiruçu, M.; Latado, A. L.; Pinto, J. C. Internal Report, Polibrasil Resinas SA, Camaçari—BA, 1999 (in Portuguese).
16. Current Trends for the Polypropylene Business; Internal Report, Polibrasil Resinas SA, Camaçari—BA, 1999.
17. U.S. Patent 3032510, Esso Res. & Eng. Co., 1962.
18. U.S. Patent 3424774, Esso Res. & Eng. Co., 1969.
19. Tonelli, A. E. NMR Spectroscopy and Polymer Microstructure: The Conformational Connection; VCH: New York, 1991.
20. Phan, Q.; Petiaud, R.; Waton, H.; Darricades, M. F. L. Proton and Carbon NMR Spectra of Polymers; Penton Press: London, 1991.
21. Gardner, K.; Parsons, I. W.; Haward, R. N. J Polym Sci A Polym Chem 1978, 16, 1683–1696.
22. Kim, I.; Choi, H. K.; Kim, J. H.; Woo, S. I. J Appl Polym Sci 1994, 52, 1739–1750.
23. Dusseault, J. J. A.; Hsu, C. C. J Appl Polym Sci 1993, 50, 431–447.
24. Ross, P. J. Taguchi Techniques for Quality Engineering, 2nd ed.; McGraw-Hill: New York, 1996.
25. Samson, J. J. C.; Bosman, P. J.; Weickert, G.; Westerterp, K. R. J Polym Sci A Polym Chem 1999, 37, 219–232.
26. Moreira, M. Internal Report, Polibrasil Resinas SA, Camaçari—BA, 1999 (in Portuguese).
27. Ystenes, M. J Catal 1991, 129, 383–392.
28. Ystenes, M. Makromol Chem Macromol Symp 1993, 66, 71–80,
29. Pinto, J. C. Macromol Theory Simul, in press.
30. Kissin, Y. V. Makromol Chem Macromol Symp 1993, 66, 83–94.

31. Soares, J. B. P.; Abbott, R. F.; Willis, J. N.; Liu, X. Macromol Chem Phys 1996, 197, 3383–3396.
32. Cerqueira, H. S.; Rawet, R.; Pinto, J. C. Appl Cat A Gen 1999, 181, 209–220.
33. Pinto, J. C. ESTIMA—A Software for Parameter Estimation and Experimental Design. User′s Guide, PEQ/COPPE/UFRJ, Rio de Janeiro—RJ, 1999.
34. Nele, M.; Collins, S.; Dias, M. L.; Pinto, J. C. Macromolecules, 2000, 33, 7249–7260.
35. Kissin, Y. V. Isospecific Polymerization of Olefins; Springer-Verlag: New York, 1985.
36. Rishina, L. A.; Vizen, E. I.; SosnovsKaja, L. N.; Dyachkovsky, F. S. Eur Polym J 30, 1994, 1309–1313.
37. Jaber, I.; Fink, G. Makromol Chem 1989, 190, 2427–2436.
38. Estenoz, D. A.; Chiovetta, M. G. Polym Eng Sci 1996, 36, 2208–2228.
39. Estenoz, D. A.; Chiovetta, M. G. Polym Eng Sci 1996, 36, 2229–2240.
40. Ferrero, M. A.; Chiovetta, M. G. Polym Eng Sci 1991, 31, 904–911.
41. Keii, T. Kinetics of Ziegler-Natta Polymerization; Kodansha Scientific Books: Tokyo, 1972.
42. Madkour, T. M.; Mark, J. E. J Polym Sci B Polym Phys 1997, 35, 2757–2764.
43. Pinto, J. C. SIMULPOL 3.0—Software for Simulation of Slurry and Bulk Propylene Polymerizations—The User's Guide; Internal Report, Polibrasil Resinas SA, Camaçari—BA, 1999.
44. Mattos Neto, A. G.; Pinto, J. C. Chem Eng Sci, in press.